치의과학박사 학위논문

The study of flexural strength and shear bond strength with surface analysis of 3D-printed 4 mol% yttria-stabilized tetragonal zirconia

3차원 프린팅으로 제작된 4몰 이트리아 안정화 지르코니아의 굴곡파절강도 및 표면 분석을 동반한 전단결합강도의 연구

2023 년 8 월

서울대학교 대학원

치의과학과 치과보철학 전공

경 규 영

The study of flexural strength and shear bond strength with surface analysis of 3D-printed 4 mol% yttria-stabilized tetragonal zirconia

지도 교수 허 성 주

이 논문을 경 규 영 박사학위논문으로 제출함

2023 년 5 월

서울대학교 대학원

치의과학과 치과보철학 전공

경 규 영

경규영의 박사학위논문을 인준함

2023 년 7 월

위 원 장	곽 재 영 (인)
부위원장	허 성 주 (인)
위 원	김 성 균 (인)
위 원	안 진 수 (인)
위 원	김 형 섭 (인)

The study of flexural strength and shear bond strength with surface analysis of 3D-printed 4 mol% yttria-stabilized tetragonal zirconia

2023

Kyu-Young Kyung, D.D.S., M.S.D

Department of Prosthodontics, Graduate School, Seoul National University

*(Directed by Professor **Seong-Joo Heo**, D.D.S., M.S.D., Ph.D.)*

Abstract

The study of flexural strength and shear bond strength with surface analysis of 3D-printed 4 mol% yttria-stabilized tetragonal zirconia

Kyu-Young Kyung, D.D.S., M.S.D.

Department of Prosthodontics, Graduate School, Seoul National University

(Directed by Professor Seong-Joo Heo, D.D.S., M.S.D., Ph.D.)

***Purpose**:* This study aimed firstly to evaluate the flexural strength of 3D-printed 4 mol% yttria-stabilized tetragonal zirconia (4Y-TZP). Secondly, the shear bond strength for veneering porcelain and resin cementation was evaluated with surface analysis.

Material & methods: In the flexural strength test, a total of eighty cylindrical specimens (15 mm diameter, 1.5 mm thickness) were fabricated. Specimens were classified into four groups by fabrication method and yttria content: milled 3Y-TZP (Katana HT, Kuraray Noritake, Tokyo, Japan), 3D-printed 3Y-TZP (TZ-3Y-E, Tosoh, Tokyo, Japan), milled 4Y-TZP (Katana STML, Kuraray Noritake, Tokyo, Japan), and 3D-printed 4Y-TZP (3DMAT, Genoss, Suwon, Korea). The biaxial flexural strength test was done with the 'Piston-on-Three-Balls' method (n=15). The flexural strength

was measured, and Weibull modulus (m) and characteristic strength (σ_0) were estimated from fracture load distribution. Intact and fractured surfaces of specimens were observed with scanning electron microscopy (SEM)(n=2). The crystalline phase was identified with X-ray diffraction (XRD)(n=5).

Ninety 4Y-TZP specimens (10 mm diameter, 1.2 mm thickness) were fabricated by 3D printing and milling for the shear bond strength test. The shear bond strength test was done for veneering porcelain (with and without sandblasting) and resin cementation. Fifteen samples were assigned for each test (n=15). Porcelain was veneered to cylindrical form on the surface of 4Y-TZP specimens with feldspathic porcelain powder (CZR dentin powder, Kuraray Noritake, Tokyo, Japan). In the test for resin cementation, the surface of the specimen was treated with sandblasting, etching, and metal/zirconia primer (Metal Primer Z, GC, Tokyo, Japan) before the composite resin (Gradia Direct Anterior, GC, Tokyo, Japan) disk was cemented with self-adhesive resin cement (Rely X U200, 3M ESPE, Saint Paul, MN, USA).

Surface analysis was conducted for specimens of shear bond strength test (n=5). Surface roughness was measured by using a 3D surface confocal laser scanning microscope. In addition, surface energy was calculated from water and diiodo-methane contact angle with the Owens-Wendt & Rable-Kaelble (OWRK) method.

The statistical analyses were performed with statistical software (SPSS version 26, IBM Corp, Armonk, NY, USA). The normality of the data for each exam was evaluated with the Shapiro-Wilk test. One-way ANOVA, or the Kruskal-Wallis test, was applied for significance among groups based on the normality and the sample size. Pairwise comparison was performed with Tukey's post hoc test for one-way ANOVA or the Mann-Whitney U-test for the Kruskal-Wallis test in case a significant difference was found among groups.

Results: 3D-printed 4Y-TZP showed significantly higher flexural strength than milled 4Y-TZP ($P<.001$), while 3D-printed 3Y-TZP had significantly lower flexural strength than milled 3Y-TZP ($P<.001$). XRD analysis indicated that the tetragonal phase was the dominant phase in all groups, and some cubic phase peaks were identified.

The surface roughness of 3D-printed 4Y-TZP was significantly lower than milled 4Y-TZP ($P<.001$). Both 3D-printed and milled 4Y-TZP showed significantly higher surface roughness after being sandblasted than their initial raw state ($P<.001$), but no significant difference was observed in surface roughness between them (Sa: $P=.877$, Sq: $P=.915$).

The surface energy of 3D-printed 4Y-TZP was significantly lower than milled 4Y-TZP ($P=.008$). However, the two groups showed no significant difference in surface energy after sandblasting ($P=.056$). The surface energy of 3D-printed 4Y-TZP was significantly increased when sandblasted ($P=.008$), while milled 4Y-TZP was not significantly ($P=.095$).

In the shear bond strength test for veneering porcelain, the 3D-printed 4Y-TZP showed significantly low shear bond strength than the milled 4Y-TZP ($P<.001$). However, as in the case of surface energy, sandblasting on their surface caused no significant difference in shear bond strength between them ($P=.412$). The shear bond strength of 3D-printed 4Y-TZP was significantly increased by sandblasting ($P<.001$). In contrast, milled 4Y-TZP showed no significant increase in shear bond strength by sandblasting ($P=.116$).

No significant difference was observed in shear bond strength for resin cementation between the 3D-printed and milled 4Y-TZP when their surfaces were sandblasted ($P=.811$).

Conclusion: Within the limitations of this study, the results suggest the following conclusions.

1. The flexural strength of 3D-printed 4Y-TZP was significantly higher than milled 4Y-TZP.
2. 3D-printed 4Y-TZP showed significantly lower shear bond strength for veneering porcelain than milled 4Y-TZP due to lower surface roughness and surface energy.
3. Surface roughness and surface energy of 3D-printed 4Y-TZP significantly increased after sandblasting.
4. 3D-printed 4Y-TZP had similar shear bond strength for veneering porcelain and resin cementation with milled 4Y-TZP when they had equivalent surface roughness and surface energy with sandblasting.

Conclusively, 3D-printed 4Y-TZP could be the preferable material for zirconia restoration with clinically acceptable flexural strength and shear bond strength compared to milled 4Y-TZP.

Keywords: Y-TZP, 3D printing, Flexural strength, Shear bond strength, Surface roughness

Student Number: 2018-39754

Table of Contents

I. INTRODUCTION

Yttrium stabilized tetragonal zirconia (Y-TZP) is a commonly used dental restorative material due to its high strength, bio-compatibility, and acceptable aesthetics.[1, 2] In general, zirconia restorations are fabricated by CAD-CAM, i.e., digitally designed by computer and manufactured by milling pre-sintered zirconia blocks and sintering them.[3] Compared with conventional restorations such as gold, PFM which are processed by analog works like lost-wax casting or building up porcelain, the fabrication process of zirconia restoration is concise and automated by using CAD-CAM system.[4-6]

On the other hand, milling is the subtractive machining process of removing material from a block to create products, and that causes several inevitable disadvantages. These include the difficulty in making complex internal structures because of the limitation of tool path, waste of material, and high maintenance cost of the instrument due to wear.[7, 8]

Additive manufacturing with 3D printing is an alternative method to overcome these problems. It can fabricate precise internal structures and reduce material consumption by applying successive layers of materials in building objects. Therefore, there is an increasing number of attempts to fabricate zirconia prostheses by 3D printing instead of milling nowadays.[8, 9]

Compared with milled zirconia, 3D-printed zirconia was reported to have lower mechanical strength due to a lack of sufficient interfacial bond strength between layers.[10, 11] Recently, however, with the development of material and printing devices, some studies reported that mechanical properties of 3D-printed zirconia were comparable to those of milled zirconia except the flexural strength.[12] Even

though 3D-printed zirconia have lower flexural strength than milled zirconia, according to the latest research findings, the flexural strength of 3D-printed 3-mol% yttria-stabilized tetragonal zirconia (3Y-TZP) was reported to be higher than 500 MPa which is the minimum recommended value of monolithic ceramic for 3-unit prostheses involving molar restoration.[13-15]

Although 3Y-TZP has excellent mechanical properties, its low translucency makes it challenging to use in the aesthetic site. Thus, Y-TZP, which had a higher yttrium content, was developed to increase translucency. 5Y-TZP shows high translucency. However, since phase transformation toughening is limited due to a higher percentage of cubic phase, its flexural strength and fracture toughness are not sufficient for long-span dental prosthesis.[16, 17] 4Y-TZP, a compromise between the 3Y-TZP and 5Y-TZP shows improved translucency without a detrimental loss of mechanical properties.[18, 19] Because of these properties, 4Y-TZP has become widely used in fabricating monolithic zirconia crown.[20]

Nowadays, there has been extensive research on 3D-printed zirconia. However, most previous studies have focused on 3Y-TZP, making it necessary to investigate the properties of 3D-printed 4Y-TZP. Biaxial flexural strength and shear bond strength to veneering porcelain or resin cementation are crucial properties for zirconia restorations in clinical situations where they will experience heavy occlusal forces, especially in the molar area. Additionally, porcelain facing may be required to improve aesthetics.

Against this background, this study was designed to conduct a biaxial flexural strength test on 3D-printed 4Y-TZP compared to milled 4Y-TZP. The study also planned to compare the flexural strength test results of 3D-printed and milled 3Y-TZP to those of previous studies and to the results of 4Y-TZP.

In the preliminary study of this research[21], 3D-printed 4Y-TZP had significantly lower surface roughness and showed significantly lower shear bond strength for veneering porcelain than milled 4Y-TZP. The low surface roughness was considered the primary factor that caused the low shear bond strength in 3D-printed 4Y-TZP. Thus, this study included the surface roughened 3D-printed 4Y-TZP group with sandblasting for further study.

This study aimed firstly to assess the flexural strength of 3D-printed 4 mol% yttria-stabilized tetragonal zirconia (4Y-TZP). Secondly, the shear bond strength for veneering porcelain and resin cementation was evaluated with surface analysis. The null hypotheses for this study were: (1) There would be no significant difference in the flexural strength between 3D-printed and milled 4Y-TZP, and (2) There would be no significant difference in the shear bond strength for veneering porcelain or resin cementation and related surface characteristics between 3D-printed and milled 4Y-TZP.

II. MATERIALS AND METHODS

1. Biaxial flexural strength test

1) Specimen preparation

Twenty of each group, a total of eighty cylindrical specimens with a diameter of 15 mm and a thickness of 1.5 mm, were fabricated from 4Y and 3Y-TZP using 3D printing and CAD-CAM milling methods. The test group consisted of 3D-printed 4Y-TZP specimens (Group PZ4), while the control group consisted of milled 4Y-TZP specimens (Group MZ4). Additionally, 3D-printed (Group PZ3) and milled 3Y-TZP specimens (Group MZ3) were prepared as reference groups in evaluating the flexural strength of 4Y-TZP specimens. Fifteen specimens were assigned to the biaxial flexural strength test (n=15). Five specimens were subjected to X-ray diffraction (XRD) and scanning electron microscopy (SEM) analysis (n=5). The materials' details and usage in the biaxial flexural strength test are summarized in Table 1.

Table 1. The details of the materials used in biaxial flexural strength test.

Group	MZ (Milling)				PZ (3D Printing)			
Subgroup	MZ3		MZ4		PZ3		PZ4	
Classification by Y_2O_3 (%)	3Y-TZP		4Y-TZP		3Y-TZP		4Y-TZP	
Materials	Katana HT		Katana STML		TZ-3Y-E		3DMAT*	
Manufacturer	Kuraray Noritake, Tokyo, Japan				Tosoh, Tokyo, Japan		Genoss, Suwon, Korea	
Fabrication Process	Dry Milling by 5-Axis milling machine (ZX-5SD, Manix, Anseong, Korea)				SLA-type 3D printer Horizontal printing (Veltz SLA, Hephzibah, Incheon, Korea)			
Composition (wt %)	ZrO_2 + HfO_2	90 - 95 %	ZrO_2 + HfO_2	88 - 93 %	ZrO_2	NP	ZrO_2	82-94 %
					HfO_2	≤ 5 %	HfO_2	≤ 5 %
	Y_2O_3	5-8 %	Y_2O_3	7-10 %	Y_2O_3	5.2±0.5 %	Y_2O_3	6-8 %
	Other oxide	≤ 2 %	Other oxide	≤ 2 %	Molding aid component	NP	Molding aid component	≤ 5 %
Size (mm)	Φ: 15 mm / h: 1.5 mm							
Sample (n)	Biaxial flexural strength test (15), XRD / SEM (5)							

NP, Not provided; *: Not commercially available

2) Measurement of the flexural strength

The flexural strength was measured with the biaxial flexural strength test by using the 'Piston-on-Three-Balls' method (Fig. 1). The study design followed the guidelines specified in ISO 6872:2015.[22]

A cylindrical shape specimen with a 15mm diameter and 1.5mm thickness was supported by three steel balls arranged equally 120° apart from each other in a circle with a diameter of 12mm. The load was applied using a 1.0 mm diameter flat-end piston attached to a universal testing machine (TCK-K500, Testone, Busan, Korea) with a 5kN load cell at a rate of crosshead speed of 0.5mm/min on the center of the specimen until fracture occurred.

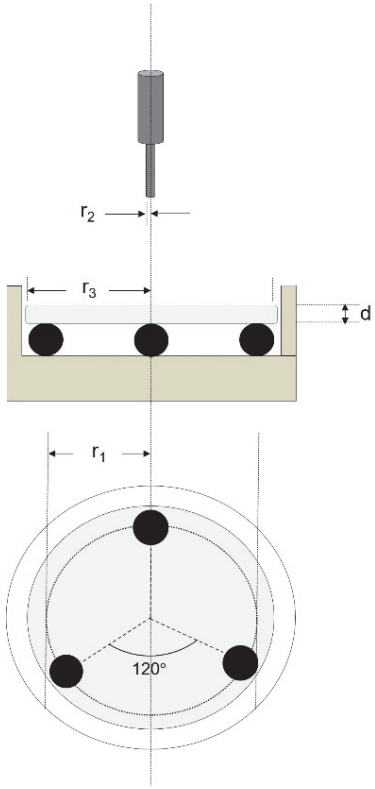

$$\delta = -0.2387\, P\, (X-Y) / d^2$$

$$X = (1+\nu) \ln (r_2/r_3)^2 + [(1-\nu)/2]\, (r_2/r_3)^2$$

$$Y = (1+\nu)\, [1+\ln (r_1/r_3)^2] + (1-\nu)\, (r_1/r_3)^2$$

δ : Flexural strength (MPa)

P : Maximum load at fracture occurred (N)

ν : Poisson's ratio (0.25)

r_1 : The radius of the support circle

r_2 : The radius of the load area of a piston

r_3 : The radius of the specimen

d : The thickness of the specimen

Figure 1. A schematic diagram of the biaxial strength test.

The flexural strength was calculated from the load at fracture with the presented formulas.

3) Weibull Analysis

Weibull modulus (m) and characteristic strength (σ_0) were estimated from fracture load distribution by using Weibull statistics and unweighted linear regression analysis. In the Weibull distribution, the probability (P_f) that a material with flexural strength (σ) would fracture at stress below this was given with the formula (1), the cumulative distribution function.

(1) $P_f = 1 - e^{-(\frac{\sigma}{\sigma_0})^m}$

Formula (1) could be converted to linear form (y = am+b) as formula (2)

(2) $ln\left[ln\left[\frac{1}{1-P_f}\right]\right] = -m\ ln\ \sigma_0 + m\ ln\ \sigma$

Where $y = ln\left[ln\left[\frac{1}{1-P_f}\right]\right]$, $a = ln\ \sigma$, $b = -m\ ln\ \sigma_0$.

The cumulative failure probability (Pi) for the strength of that specimen with rank i (where the samples were ranked from weakest, i = 1, to most robust, i = N) fractured could be obtained from formula (3), the probability estimators suggested by Blom.[23]

(3) $P_i = \frac{i-0.375}{N+0.25}$

Unweighted linear regression was done with the measured flexural strengths (σ) and values of P_i. Then, using the result of linear regression and formula (2), Weibull modulus (m) and characteristic strength (σ_0) were obtained.[24]

Graph plotting and data processing was conducted with data analysis and graphing software (OriginPro, v2023, OriginLab, Northampton, MA, USA).

4) SEM Analysis

The surface of the intact and fractured specimens (n=2) of the biaxial strength test was observed with SEM (Apreo S, Thermo Fisher Scientific, Waltham MA, USA). Specimens were gold-coated to provide conductivity and improve the image's resolution, and the accelerating voltage was 10kV. Images were obtained at magnifications of 1,000, 5,000, and 20,000 for the intact specimens, while fractured specimens were at 200, 5,000, and 20,000.

5) XRD Analysis

The crystalline phase was investigated with XRD (AERIS, Malvern Panalytical, Malvern, UK). The specimens (n=5) were scanned between $2\theta = 10 - 90^{\circ}$with Cu Kα radiation ($\lambda K\alpha_1$ = 1.5406 Å, $\lambda K\alpha 2$ = 1.5444 Å, $K\alpha_2/K\alpha_1$=0.5). The Joint Committee on Powder Diffraction Standards - International Centre for Diffraction Data (JCPDS-ICDD) card was used in identifying the crystalline phase by comparing it with the diffractogram. (Monoclinic: 00-037-1484[25], Tetragonal: 00-014-0534[26], Cubic: 00-027-0997[27]).

2. Shear bond strength test with surface analysis

1) Specimen preparation

Ninety 4Y-TZP samples with 10 mm diameter and 1.2 mm thickness were fabricated with milling for the control group and 3D printing for the test group. The shear bond strength test was done for porcelain veneering (with and without sandblasting on the 4Y-TZP surface) and resin cementation. Fifteen samples were assigned for each test (n=15). The sample number was determined following ISO 29022:2013.[28] Five specimens were randomly selected from each group for surface analysis during the test for veneering porcelain. Surface roughness and surface energy were measured with these specimens. A detailed overview of the materials is summarized in Table 2.

Table 2. The details of the materials in the shear bond strength test.

Group		MZ (Milling)		PZ (3D Printing)	
Subgroup		MZ4R	MZ4S	PZ4R	PZ4S
Materials		Milled 4Y-TZP (Katana STML)		3D printed 4Y-TZP (3DMAT)	
Size (mm)		Φ : 10 mm / h : 1.2 mm			
Surface Treatment		Raw	Sandblasted	Raw	Sandblasted
Sample (n)	Resin cementation	.	15	.	15
	Veneering porcelain	15	15	15	15
	Surface Analysis	5*	5*	5*	5*

* Five were randomly selected from specimens of the shear bond strength test.

2) Surface Analysis

A. Measurement of Surface Roughness

The specimens' 3D surface roughness (Sa, Sq) was measured with a 3D surface confocal laser scanning microscope (LSM 800, Carl Zeiss, Oberkochen, Germany). Five specimens were evaluated for each group, with measurements taken from five different areas per specimen: one at the center and four circumferential areas. The measurements were conducted on both untreated specimens and sandblasted specimens. The sandblasting process involved using 50μm Al_2O_3 particles at a pressure of 2.5 bar for 15 seconds, with a distance of 10mm.

B. Evaluation of Surface Energy

Surface energy was calculated from contact angles of water and diiodo-methane by the Owens-Wendt & Rable-Kaelble (OWRK) method. [29, 30]

Water and diiodo-methane contact angles were measured by a drop shape analyzer (DSA-100, KRUSS GmbH, Hamburg, Germany) for five samples in each group. The drop size was 10ul for water and 2ul for diiodo-methane.

3) Veneering porcelain to zirconia

3D-printed and milled 4Y-TZP specimens with 10 mm diameter and 1.2 mm thickness were veneered with porcelain in a cylindrical shape of 8±0.1 mm diameter and 2 mm thickness. Half were veneered without surface treatment (n=15) in each group, and the other half were sandblasted on the surface (n=15) before veneering porcelain.

Ring shape silicon mold with a size of 10mm inner diameter and 3mm thickness was used to consistently build up feldspathic porcelain powder (CZR dentin powder, Kuraray Noritake, Tokyo, Japan) to cylindrical form on zirconia specimen. Then, it was fired in the furnace (Programat P310, Ivoclar-Vivadent, Vaduz, Liechtenstein) according to the manufacturer's instructions. The marginal area of the sintered specimen was polished using a fine shoulder highspeed diamond bur with a 1mm diameter (8836KR-010, Komet, Lemgo, Germany) to adjust the size and to remove surface irregularity that occurred by porcelain shrinkage in firing.

The diameter of the veneered porcelain was measured using digital vernier calipers (5110-300, Wenzhou Sanhe Measuring Instrument Co., Wenzhou, China) in four different axes: 0°-180°, 45°-225°, 90°-270°, and 135°-315°. The average of the measured diameters from all four axes was used in calculating the bonded surface area.

Then, the porcelain veneered 4Y-TZP specimen was embedded in PMMA resin (ProBase Cold, Ivoclar-Vivadent, Vaduz, Liechtenstein) with a size of 20mm x 20mm x 20mm to be mounted in a universal testing machine (TCK-K500, Testone, Busan, Korea).

4) Resin cementation to zirconia

One side of the 4Y-TZP specimen was protected using commercially available clear tape (Scotch tape, 3M, Saint Paul, MN, USA) when embedded in PMMA resin for being mounted in a universal testing machine. After the complete polymerization of PMMA resin, the clear tape was removed. Any surface irregularities around the exposed surface of 4Y-TZP were removed and polished.

The 4Y-TZP specimen underwent the following surface treatment procedures before cementation of the composite resin (Gradia Direct Anterior, GC, Tokyo, Japan) with self-adhesive resin cement (Rely X U200, 3M ESPE, Saint Paul, MN, USA). It was air-abraded using 50 μm Al_2O_3 particles at 2.5 bar pressure for 15 seconds at a 10mm distance. Then, 37% phosphoric acid was applied for 15 seconds, followed by thorough water rinsing and drying. Finally, metal/zirconia primer (Metal Primer Z, GC, Tokyo, Japan) was applied and dried.

A silicon ring was placed around the bonding surface and secured with clear tape for stable positioning of the composite resin disk during cementation. The composite resin disk, with an 8mm diameter and 2mm thickness, was then cemented onto the treated 4Y-TZP surface with the self-adhesive resin cement under a constant 1.96N load, achieved by applying a 200g weight.

5) Measurement of Shear Bond Stress

Prior to measurement, all specimens were kept in the water bath at 37℃ for 24 hours and thermo-cycled between 5℃ and 55℃ with a 30-second dwell time. A universal testing machine (TCK-K500, Testone, Busan, Korea) with a knife-edge chisel was used to apply shear load on the bonding interface at a cross-head speed of 1mm/min until failure. The shear load at which failure occurred (N) was measured, and the shear bond strength (MPa) was calculated by dividing that value by the bonded surface area (mm^2). Weibull Analysis was done from failure load distribution. Fractured surfaces were observed to identify the failure mode using an x10 stereo zoom microscope (300IIX10, Ziecor International, Inc., Tokyo, Japan). Failure modes of specimens were classified as cohesive failure when the fracture occurred within the porcelain or resin cement, adhesive failure at the interface between the specimen and porcelain or resin cement, and mixed failure, which consists of cohesive and adhesive failure.

A schematic diagram of the shear bond strength test is illustrated in Figure 2.

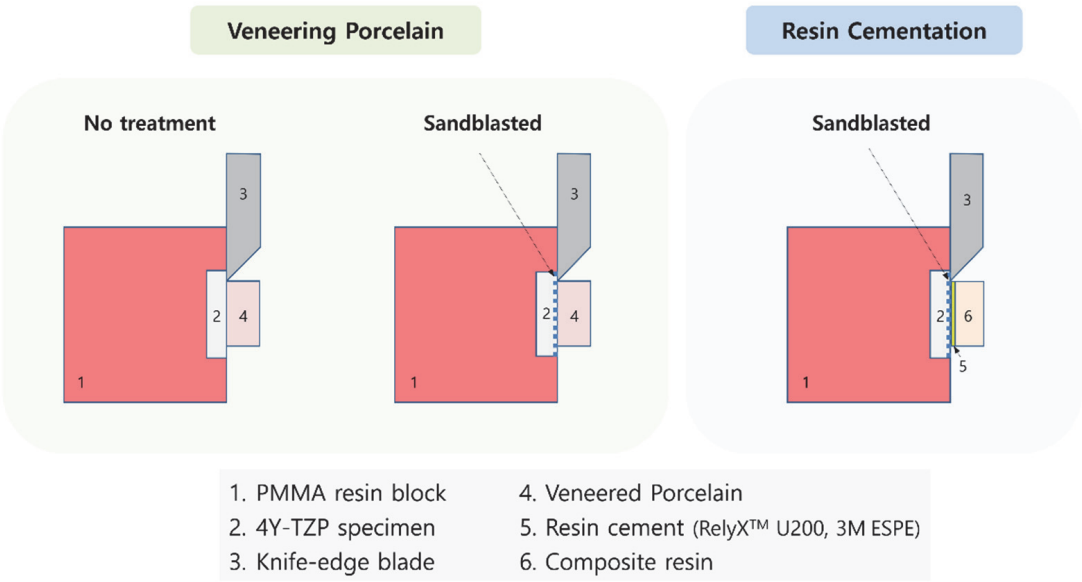

Figure 2. A schematic diagram of the shear bond strength test

3. Statistical Analysis

The Shapiro-Wilk test was used to evaluate the normality of the dataset for each exam. In the flexural strength test, either one-way ANOVA or the Kruskal-Wallis test was used to test for significance among groups (Group MZ3, MZ4, PZ3, PZ4), depending on whether the normality requirement was met. If a significant difference was found among groups, pairwise comparison was performed using Tukey's post hoc test for ANOVA or the Mann-Whitney U-test for the Kruskal-Wallis test.

In the shear bond strength test of resin cementation, the statistical significance between the test (PZ4S) and control group (MZ4S) was evaluated with an independent t-test or Mann-Whitney U-test, depending on the normality of the dataset. In comparing the shear bond strength of veneering porcelain and surface characteristics (contact angle, surface energy, surface roughness) among groups (MZ4R, MZ4S, PZ4R, PZ4S), one-way ANOVA or Kruskal-Wallis test was used, depending on the normality of the dataset and the sample size of each group. Tukey's post hoc test was used for ANOVA, and the Mann-Whitney U-test was used for the Kruskal-Wallis test in case of significance among the groups. Statistical analyses were performed with statistical software (IBM SPSS, v26; IBM Corp, Armonk, NY, USA).

III. RESULTS

1. Biaxial flexural strength test

1) Flexural strength & Weibull Analysis.

One-way ANOVA was applied for significance among groups since the normality assumption was satisfied. There was a significant difference among the groups in the flexural strength ($P<.001$), and thus Tukey's post hoc test was performed to identify specific pairs of groups that were significantly different. Milled 3Y-TZP specimens (MZ3) showed the highest strength and were significantly higher than other groups ($P<.001$). There was no significant difference in the flexural strength between the 3D-printed 3Y-TZP (PZ3) and 4Y-TZP (PZ4) specimens ($P=.119$). Milled 4Y-TZP specimens (MZ4) showed the lowest strength and were significantly lower than other groups ($P<.001$). The specimens with higher flexural strength were fractured into more segments (Fig. 3). The box and Weibull probability plot of the biaxial strength test were presented in Figures 4 and 5. Group MZ3 showed the highest Weibull modulus, while group PZ3 showed the lowest Weibull modulus. The overall study results and statistical analysis of the biaxial flexural strength test were summarized in Tables 3 and 4.

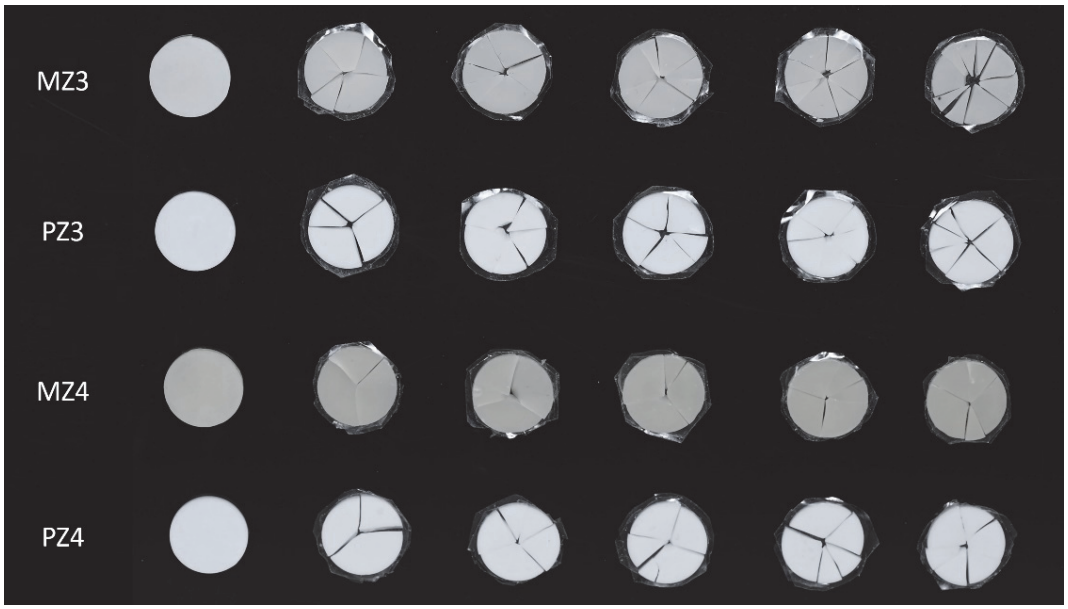

Figure 3. The representative images of fractured specimens in a biaxial flexural strength test. A higher biaxial flexural strength led to an increased number of fractured pieces. MZ3, Milled 3Y-TZP; PZ3, 3D-printed 3Y-TZP; MZ4, Milled 4Y-TZP; PZ4, 3D-printed 4Y-TZP.

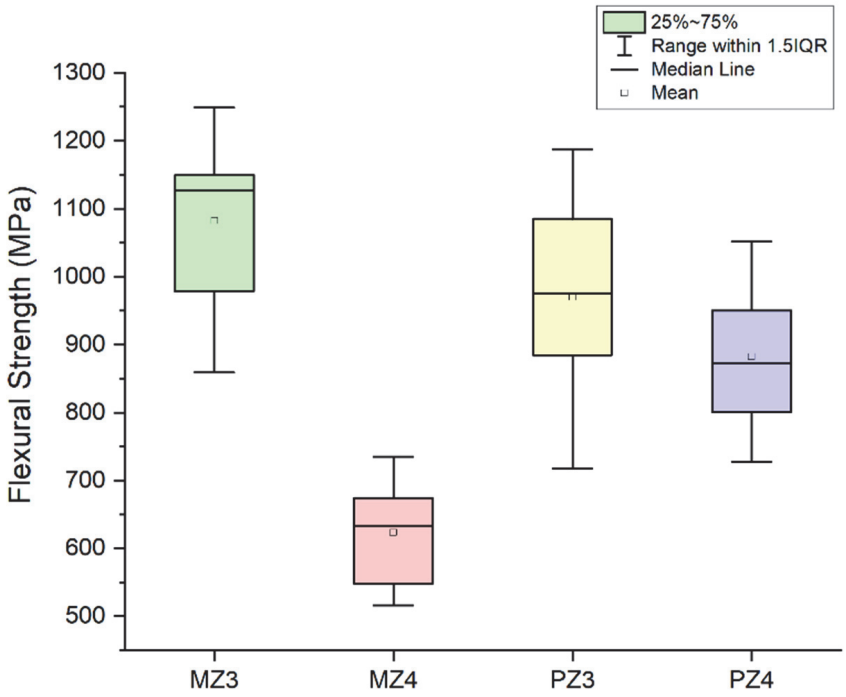

Figure 4. A box plot of the biaxial flexural strength test.

IQR, Interquartile range; MZ3, Milled 3Y-TZP; PZ3, 3D-printed 3Y-TZP; MZ4, Milled 4Y-TZP; PZ4, 3D-printed 4Y-TZP.

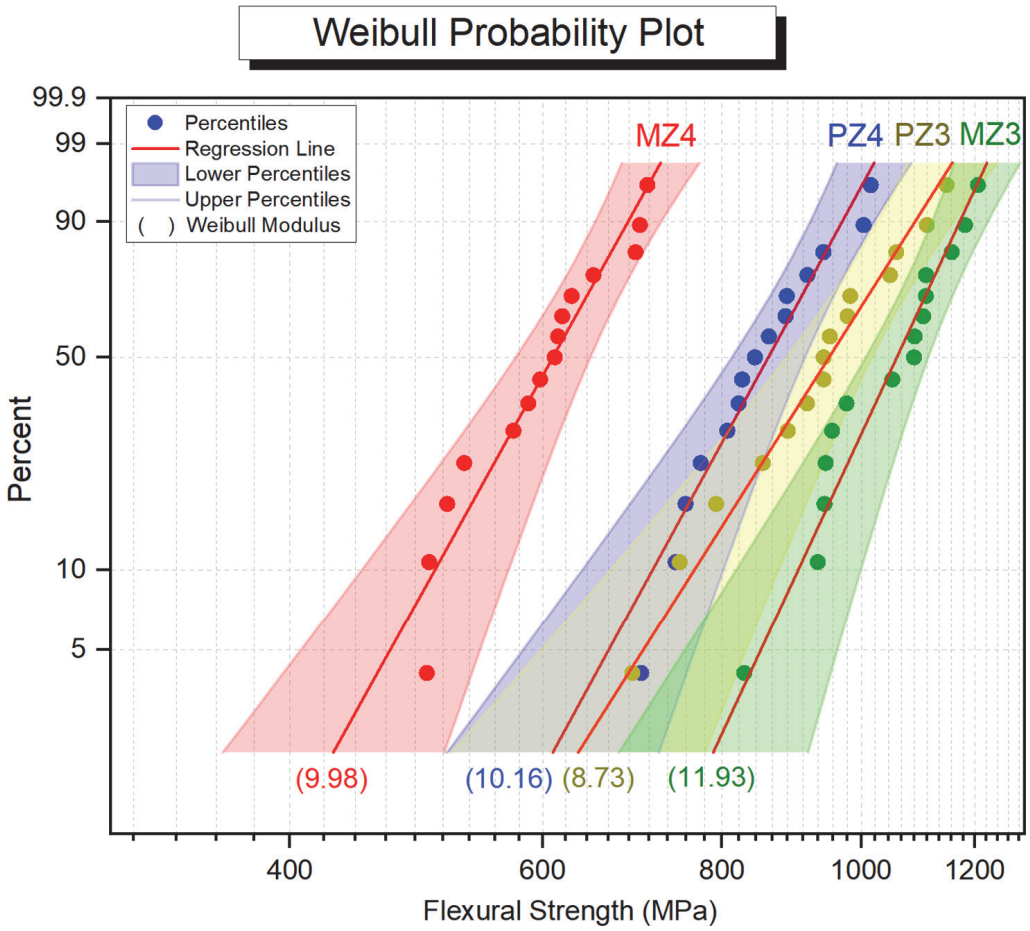

Figure 5. A Weibull probability plot of the biaxial flexural strength test

Unweighted linear regression was done for the measured flexural strengths and values of the cumulative failure probabilities. The Weibull modulus was estimated from the slope of the regression line (red line in each group), which describes variability in measured material strength.[24] MZ3, Milled 3Y-TZP; PZ3, 3D-printed 3Y-TZP; MZ4, Milled 4Y-TZP; PZ4, 3D-printed 4Y-TZP.

Table 3. The study results of the biaxial strength test.

Group	MZ (Milling)		PZ (3D Printing)		*P*
Subgroup	MZ3	MZ4	PZ3	PZ4	
Flexural Strength (MPa)	1045.3 ±108.7 [A]	602.1 ±70.3 [C]	936.8 ±128.6 [B]	852.4 ±92.0 [B]	< .001
Characteristic Strength* (MPa)	1091.86	632.57	990.56	893.17	-
Weibull Modulus**	11.93	9.98	8.73	10.16	-

* The characteristic strength in Weibull analysis is the strength value at which the cumulative failure probability equals 63.2%.[31]

** The Weibull modulus is the distribution shape parameter of the Weibull distribution to describe variability in measured material strength.[31]

Table 4. Multiple comparison of groups with Tukey's post hoc test.

Pair	MZ3-MZ4	MZ3-PZ3	MZ3-PZ4	MZ4-PZ3	MZ4-PZ4	PZ3-PZ4
P	.000*	.026*	.000*	.000*	.000*	.119

*: $P < .05$ for significance

2) SEM image

The surface of the tested specimen of each group was observed with SEM (Fig. 6). Milled Y-TZP specimens showed evenly spaced straight lines and continuously aligned small half circles between lines at low magnification (x1,000). In contrast, 3D-printed specimens showed very smooth and consistent surfaces. At high magnification (x20,000), some grains were observed in milled Y-TZP specimens. Compared with 4Y-TZP specimens, 3Y-TZP specimens showed a smaller grain size, and grains were aligned more densely.

The low magnification (x200) SEM images of the cross-sectional surface of the fractured specimens revealed that the area adjacent to the impacted site was rougher than the opposite site. At high magnification (x20,000), grains were observed in 3D-printed specimens. In both 3D-printed and milled specimens, the 3Y-TZP specimen showed a smaller grain size and dense structure (Fig. 7).

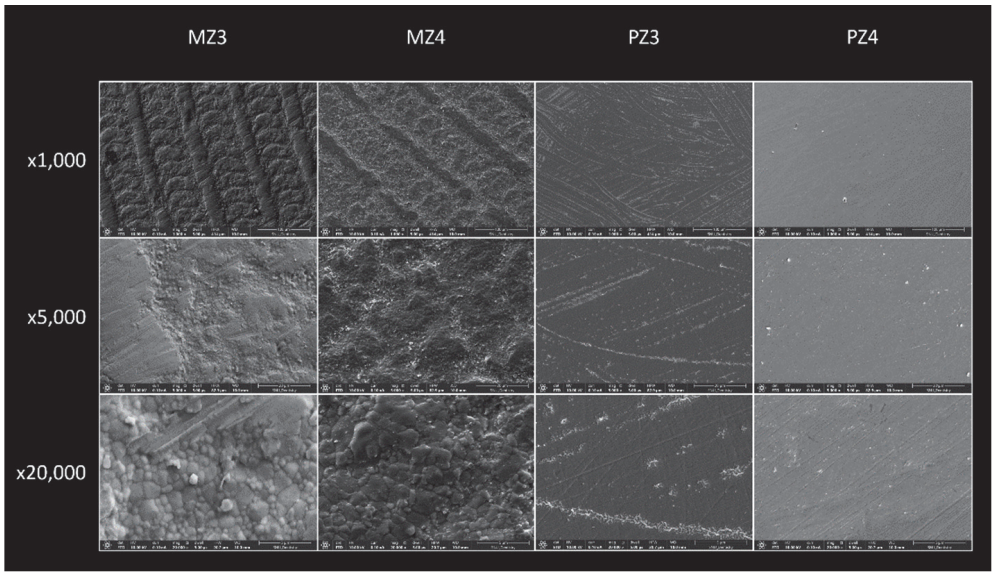

Figure 6. SEM images of the surface of the tested specimens of each group. MZ3, Milled 3Y-TZP; PZ3, 3D-printed 3Y-TZP; MZ4, Milled 4Y-TZP; PZ4, 3D-printed 4Y-TZP.

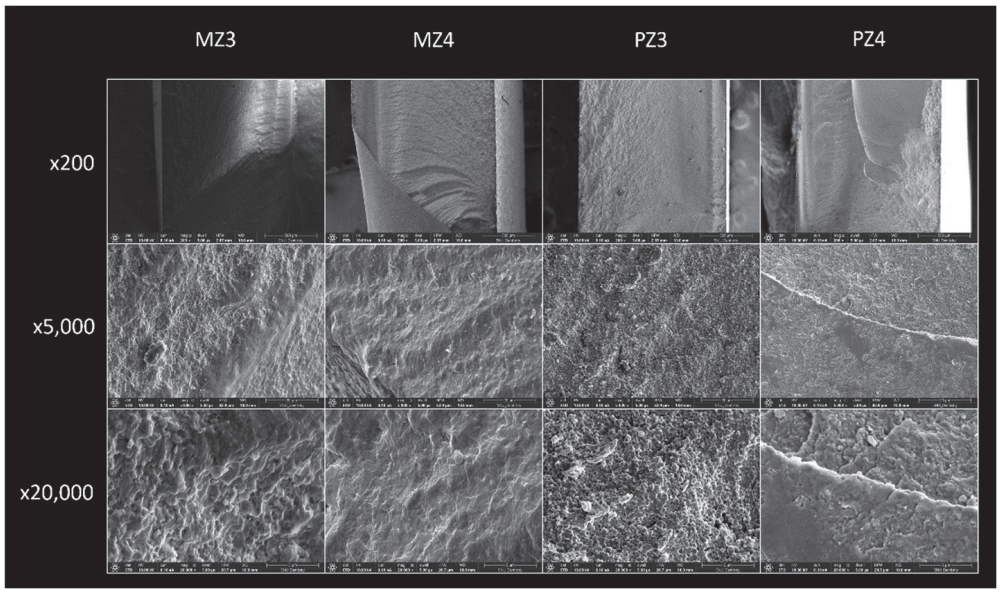

Figure 7. SEM images of the cross-sectional surface of fractured specimens in the biaxial strength test. MZ3, Milled 3Y-TZP; PZ3, 3D-printed 3Y-TZP; MZ4, Milled 4Y-TZP; PZ4, 3D-printed 4Y-TZP.

3) XRD Analysis

XRD patterns of the tested specimens of each group were obtained (Fig. 8). The tetragonal phase was the dominant phase in all groups, and some cubic phase peaks were identified. The monoclinic phase peak (=11, 2θ=28.175) was weakly observed only in milled 3Y-TZP specimens.

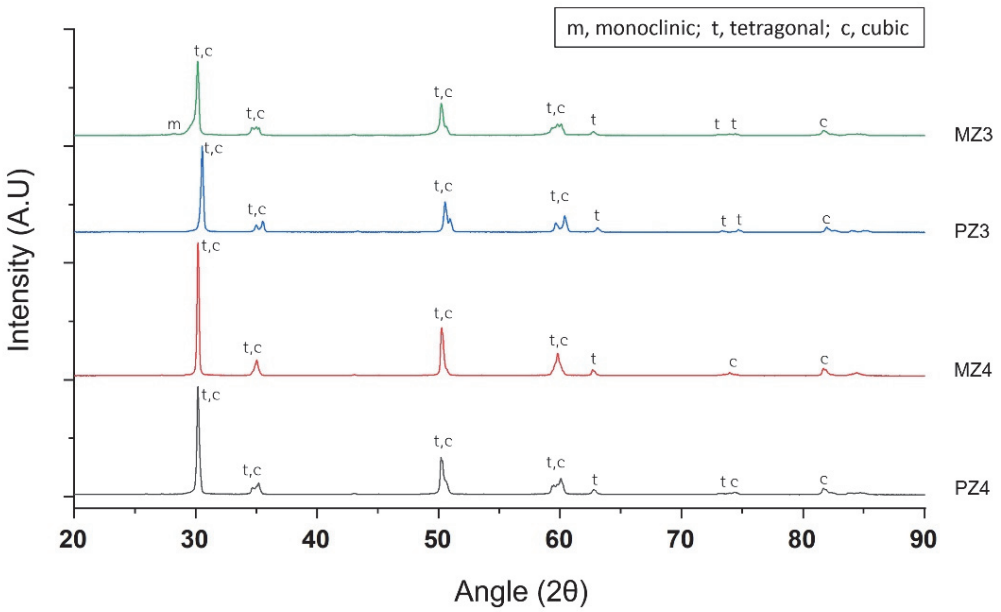

Figure 8. The XRD pattern of the tested specimens of each group

MZ3, Milled 3Y-TZP; PZ3, 3D-printed 3Y-TZP; MZ4, Milled 4Y-TZP; PZ4, 3D-printed 4Y-TZP.

2. Shear bond strength test with surface analysis

1) Surface Roughness

The Kruskal-Wallis test was applied to evaluate statistical differences among groups since the normality assumption was not satisfied. Pairwise comparison was performed with the Mann-Whitney U-test due to significance among groups ($P<.001$). Group PZ4R (Sa: 0.064±0.010 um, Sq: 0.099±0.068 um) showed significantly lower surface roughness than the other groups. The surface roughness of Group MZ4R (Sa: 0.358±0.130 um, Sq: 0.469±0.151 um) was significantly higher compared to Group PZ4R but lower than the sandblasted groups, namely MZ4S (Sa: 0.595±0.140 um, Sq: 0.755±0.173 um) and PZ4S (Sa: 0.582±0.062 um, Sq: 0.742±0.079 um). There was no significant difference in surface roughness between Groups MZ4S and PZ4S. Figures 9 and 10 provided representative surface images and extracted profiles obtained with a confocal laser scanning microscope.

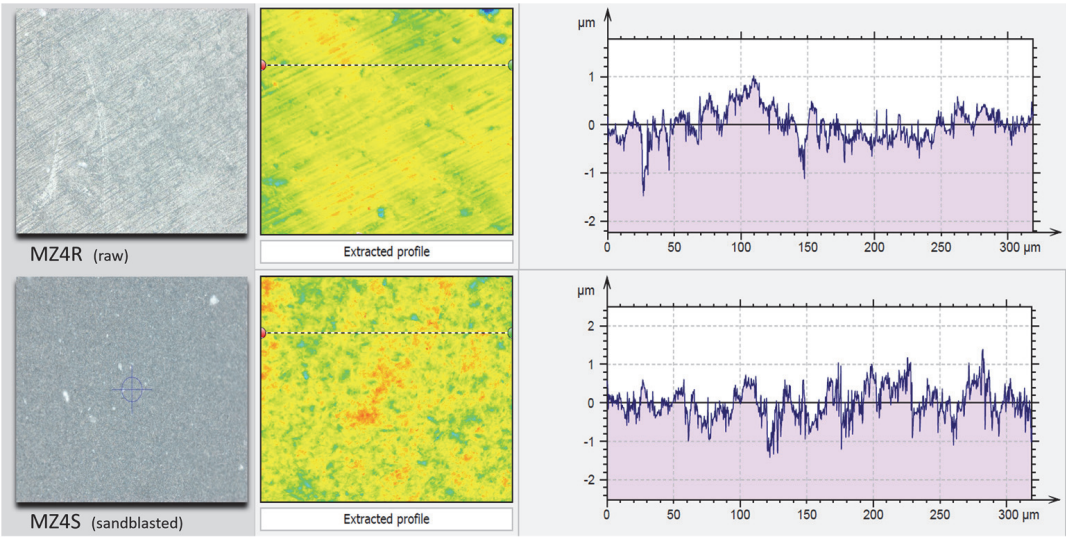

Figure 9. The confocal scanning laser microscope images and extracted profiles of milled 4Y-TZP specimens. (Group MZ4R, MZ4S)

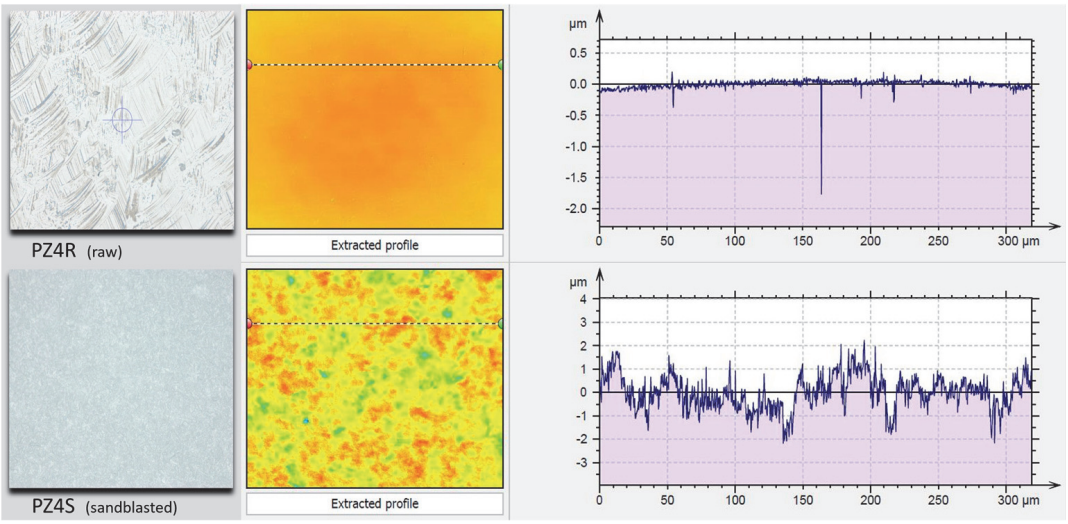

Figure 10. The confocal scanning laser microscope images and extracted profiles of 3D-printed 4Y-TZP specimens. (Group PZ4R, PZ4S)

2) Surface Wettability

The Kruskal-Wallis test was utilized to assess the statistical distinctions among groups, taking into account a small sample size (n=5). Significant differences were found among the groups in all measurements, including water contact angle (P=.002), diiodo-methane contact angle (P=.002), and surface energy (P=.004). A pairwise post hoc test using the Mann-Whitney U-test was performed for each measurement.

In water contact measurement, Group PZ4 had a significantly higher water contact angle with a mean value of 85.00±1.39° compared to the other groups. However, there was no significant difference in the mean value of water contact angle between the remaining groups, which were PZ4S (66.37±3.02°), MZ4R (59.41±4.52°), and MZ4S (58.50±4.47°).

The mean values and standard deviations of the diiodo-methane contact angle were 52.10±2.20° (Group PZ4R), 37.32±0.96° (Group PZ4S), 50.07±2.86° (Group MZ4R), and 37.56±2.54° (Group MZ4S). There was no significant difference between the groups that share the same surface treatment but differ in the fabrication process, i.e., Group PZ4R vs. Group MZ4R and Group PZ4S vs. Group MZ4S. While there was a significant difference between the groups with the same fabrication process but differed in the surface treatment, which was Group PZ4R vs. PZ4S and Group MZ4R vs. MZ4S.

The representative images of each group's water and diiodo-methane contact angle were presented in Figures 11 and 12.

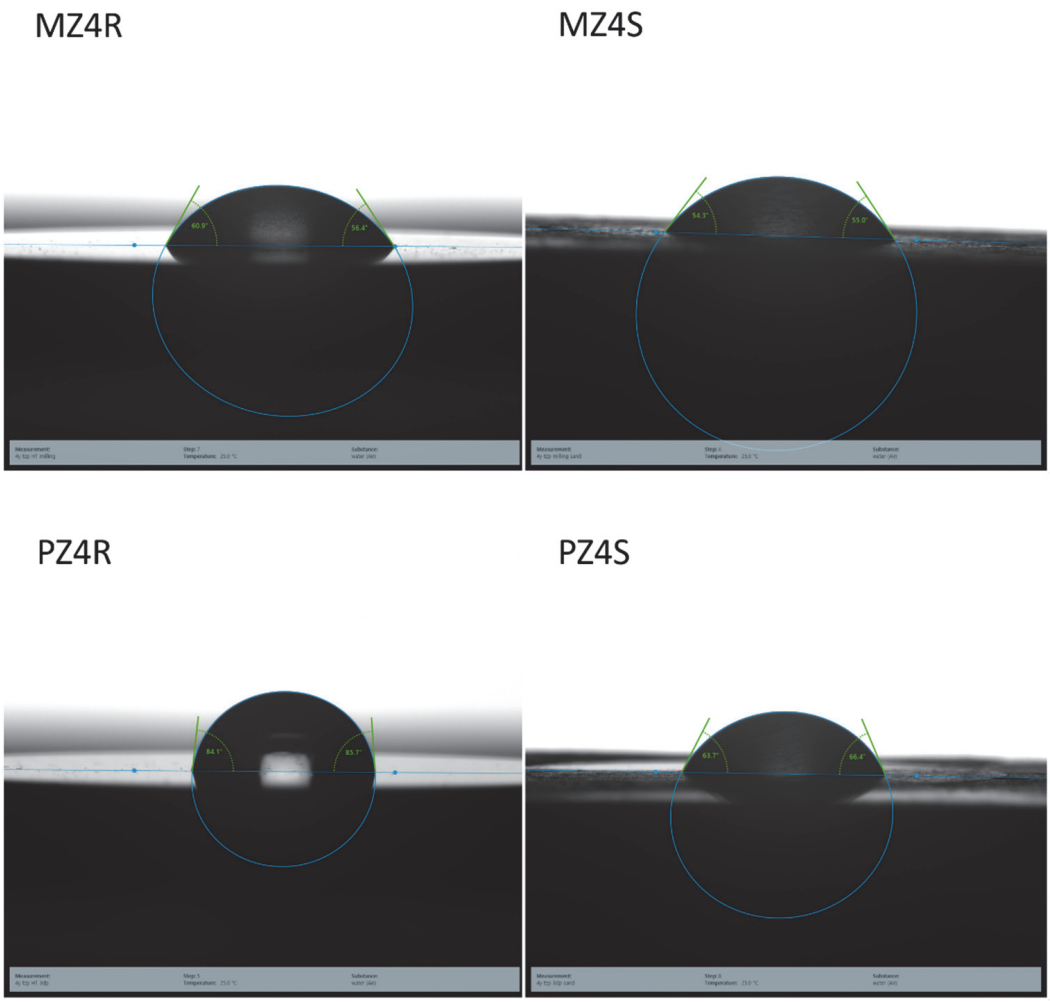

Figure 11. The representative images of the water contact angle of each group. MZ4R, Milled 4Y-TZP with a raw surface; MZ4S, Milled 4Y-TZP with sandblasted surface; PZ4R, 3D-printed 4Y-TZP with a raw surface; PZ4S, 3D-printed 4Y-TZP with sandblasted surface.

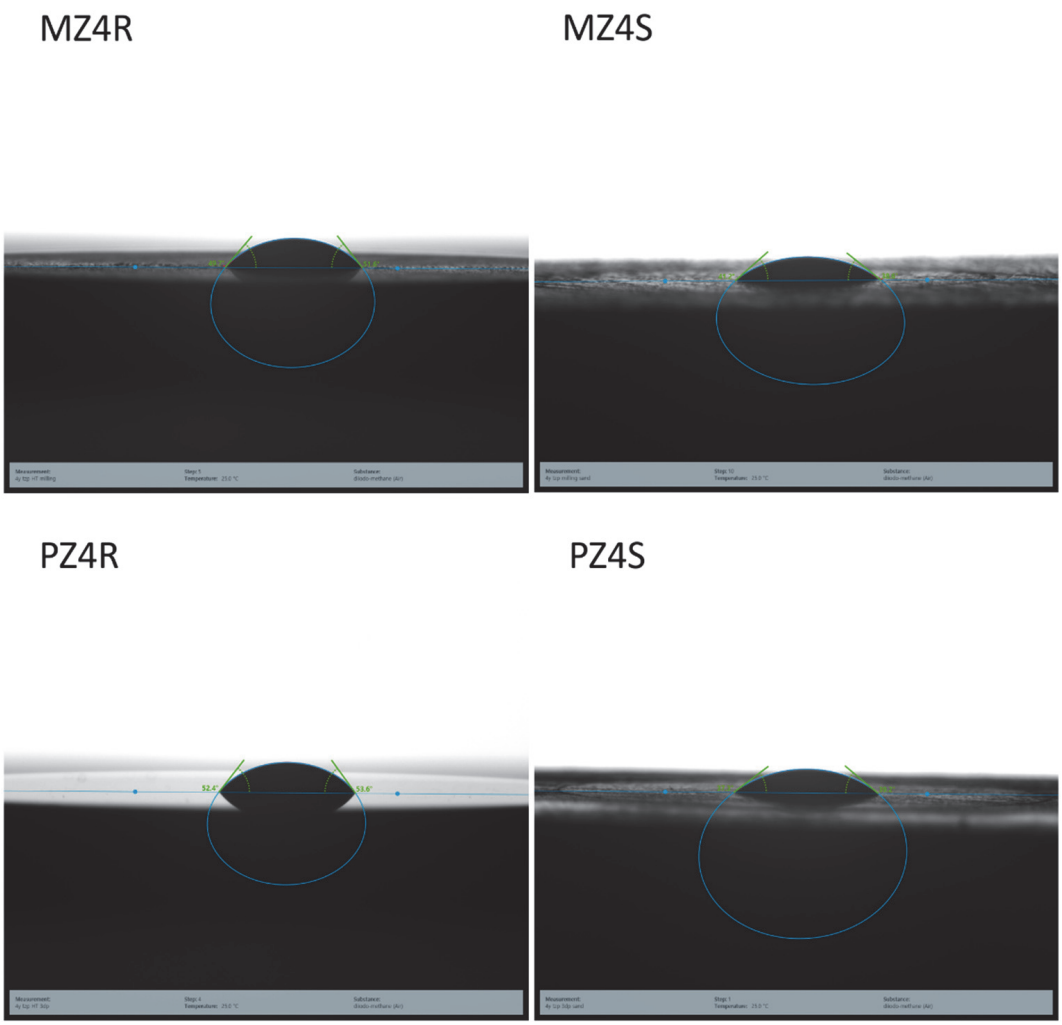

Figure 12. The representative images of the diiodo-methane contact angle of each group. MZ4R, Milled 4Y-TZP with a raw surface; MZ4S, Milled 4Y-TZP with sandblasted surface; PZ4R, 3D-printed 4Y-TZP with a raw surface; PZ4S, 3D-printed 4Y-TZP with sandblasted surface.

The surface energy was determined from the measured contact angles of water and diiodo-methane by using the Owens-Wendt & Rable-Kaelble (OWRK) method. The resulting surface energy values were 36.26±1.34 mN/m for Group PZ4R, 49.70±1.73 mN/m for Group PZ4S, 49.18±3.48 mN/m for Group MZ4R, and 53.66±3.17 mN/m for Group MZ4S. Group PZ4R showed significantly lower surface energy compared to the other groups. In contrast, there was no significant difference between the remaining groups.

3) Shear bond strength test for veneering porcelain

The Kruskal-Wallis test was used to identify the statistical differences among all four groups, including PZ4R, PZ4S, MZ4R, and MZ4S, due to violating the normality assumption in group MZ4S. A pairwise post hoc test with the Mann-Whitney U-test was performed due to significance among four groups (P<0.001). The results indicated that the shear bond strength of group PZ4R, with the lowest value of 10.75±0.85 MPa, was significantly lower than the other groups (*P*<.001). Mixed failure patterns, adhesive pattern-like but with a small portion of porcelain remnants, were observed in PZ4R. There was no significant difference in the mean shear bond strength among the remaining three groups, namely PZ4S (14.30±2.38 MPa), MZ4R (14.28±1.94 MPa), and MZ4S (15.48±2.44 MPa). Mixed failure patterns were also observed in these groups but closer to cohesive failure patterns. The box plot and Weibull probability plot of the shear bond strength test were presented in Figures 13 and 14, and overall results were summarized in Table 5.

Table 5. The study results of the shear bond strength test for veneering porcelain

Group	MZ (Milling)		PZ (3D Printing)		*P*
Subgroup	MZ4R	MZ4S	PZ4R	PZ4S	
Shear bond strength (MPa)	14.28 ±1.94^{A}	15.48 ±2.44^{A}	10.75 ±0.85^{B}	14.30 ±2.38^{A}	< 0.001
Characteristic Strength (MPa)	15.13	16.53	11.14	15.29	.
Weibull Modulus	7.99	6.29	12.97	7.00	.

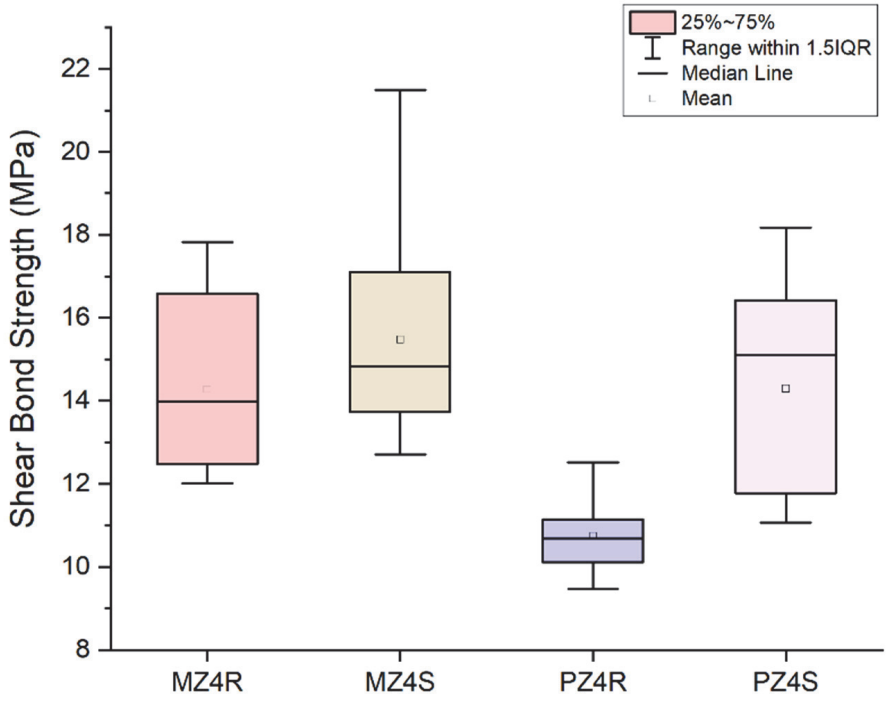

Figure 13. A box plot of the shear bond strength for veneering porcelain.

IQR, Interquartile range; MZ4R, Milled 4Y-TZP with a raw surface; MZ4S, Milled 4Y-TZP with sandblasted surface; PZ4R, 3D-printed 4Y-TZP with a raw surface; PZ4S, 3D-printed 4Y-TZP with sandblasted surface.

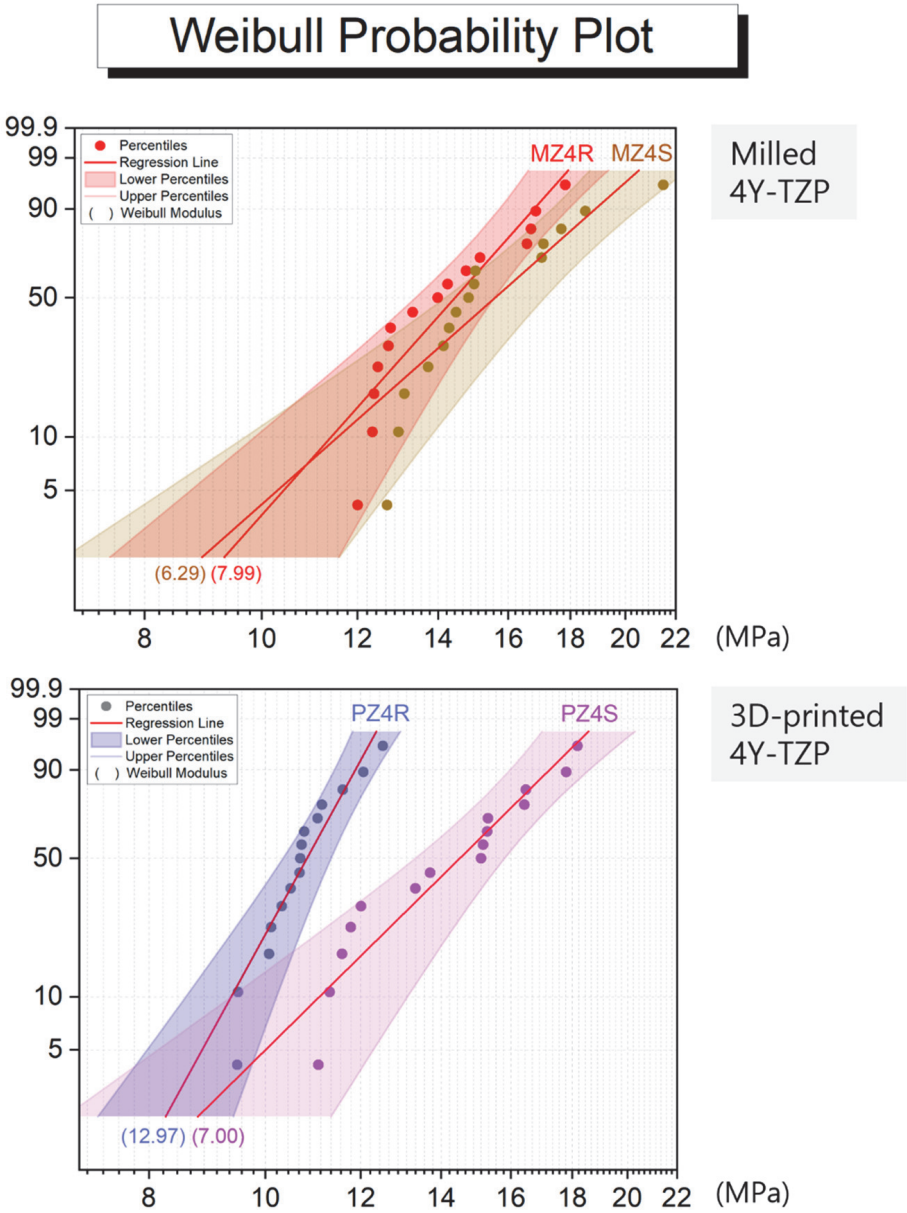

Figure 14. Weibull probability plots of the shear bond strength for veneering porcelain. MZ4R, Milled 4Y-TZP with a raw surface; MZ4S, Milled 4Y-TZP with sandblasted surface; PZ4R, 3D-printed 4Y-TZP with a raw surface; PZ4S, 3D-printed 4Y-TZP with sandblasted surface.

4) Shear bond strength test for resin cementation

An independent t-test was used to determine the statistical significance between the groups since the normality assumption was satisfied. There was no significant difference in shear bond strength between the test group (PZ4S) and the control group (MZ4S) for resin cementation (*P*=.811). The mean shear bond strength of group PZ4S was 3.33±0.98 MPa, while MZ4S's was 3.25±0.83 MPa (Fig. 15). The characteristic strength of group PZ4S was 3.68 MPa, and for group MZ4S, it was 3.56 MPa. The Weibull modulus was relatively low, with a value of 3.68 for group PZ4S and 4.39 for group MZ4S, indicating that the variability of the shear bond strength was high (Fig. 16). Mixed failure patterns were observed in the fractured surfaces for both groups, characterized by an adhesive pattern-like appearance but small remnants of resin cement remained.

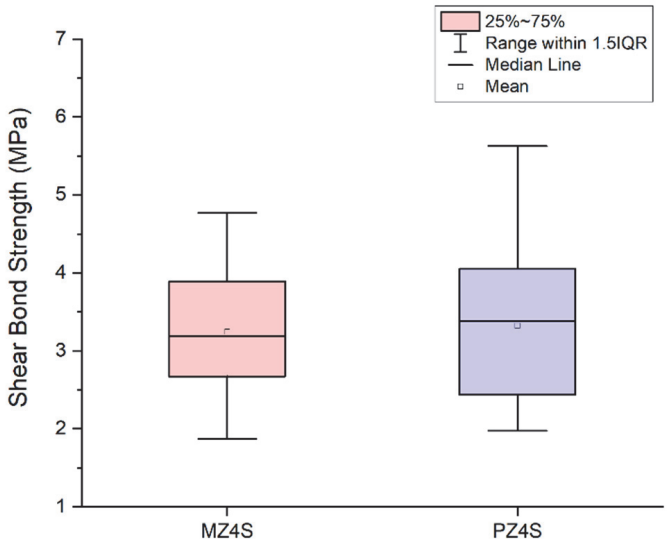

Figure 15. A box plot of the shear bond strength for resin cementation. IQR, Interquartile range; MZ4S, Milled 4Y-TZP with sandblasted surface; PZ4S, 3D-printed 4Y-TZP with sandblasted surface.

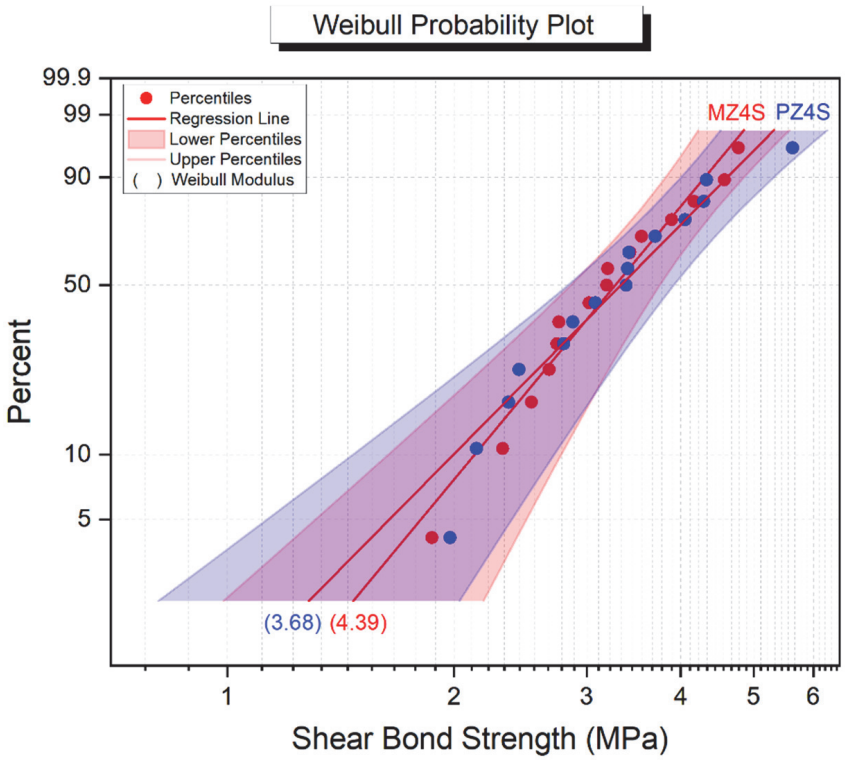

Figure 16. A Weibull probability plot of the shear bond strength for resin cementation. MZ4S, Milled 4Y-TZP with sandblasted surface; PZ4S, 3D-printed 4Y-TZP with sandblasted surface.

The surface analysis and shear bond strength test results were summarized in Table 6, and Table 7 presented detailed statistical analyses.

Table 6. The overall results of the shear bond strength test and surface analysis.

Group		MZ (Milling)		PZ (3D printing)		*P*
Subgroup		MZ4R	MZ4S	PZ4R	PZ4S	
Surface Roughness (um)	Sa	0.358 ±0.130^{B}	0.595 ±0.140^{A}	0.064 ±0.010^{C}	0.582 ±0.062^{A}	< .001
	Sq	0.469 ±0.151^{B}	0.755 ±0.173^{A}	0.099 ±0.068^{C}	0.742 ±0.079^{A}	< .001
Contact Angle (°)	Water	59.41 ±4.52^{B}	58.50 ±4.47^{B}	85.00 ±1.39^{A}	66.37 ±3.02^{B}	.002
	Diiodo-methane	50.07 ±2.86^{A}	37.56 ±2.54^{B}	52.10 ±2.20^{A}	37.32 ±0.96^{B}	.002
Surface Energy (mN/m)		49.18 ±3.48^{A}	53.66 ±3.17^{A}	36.26 ±1.34^{B}	49.70 ±1.73^{A}	.004
Shear Bond Strength (MPa)	Resin	.	3.25 ±0.83	.	3.33 ±0.98	.811
	Porcelain	14.28 ±1.94^{A}	15.48 ±2.44^{A}	10.75 ±0.85^{B}	14.30 ±2.38^{A}	< .001

Table 7. Multiple comparison of groups with the Mann-Whitney U-test.

Pair		MZ4R-MZ4S	MZ4R-PZ4R	MZ4R-PZ4S	MZ4S-PZ4R	MZ4S-PZ4S	PZ4R-PZ4S
Surface Roughness	Sa	.000*	.000*	.000*	.000*	.877	.000*
	Sq	.000*	.000*	.000*	.000*	.915	.000*
Contact Angle	Water	.841	.008*	.056	.008*	.016	.008*
	Diiodo-methane	.008*	.548	.008*	.008*	1.00	.008*
Surface Energy		.095	.008*	.841	.008*	.056	.008*
Shear bond strength of veneering porcelain		.116	.000*	.870	.000*	.412	.000*

* : $P < .05/6$ for significance

IV. DISCUSSION

1. Biaxial flexural strength test

The previous studies about 3D-printed zirconia reported that its mechanical properties were comparable to milled zirconia except for the flexural strength. Inconsistent findings were reported when examining the flexural strength of 3D-printed zirconia versus milled zirconia.[12, 32] Still, there were more studies revealed that the flexural strength of 3D-printed zirconia is not strong enough as milled zirconia.[11, 13-15] Insufficient interlayer bonding and porosity resulting from the debinding process were frequently reported as factors limiting the attainment of high flexural strength in 3D-printed zirconia.[15, 33, 34]

In this study, flexural strength tests were conducted on 3D-printed and milled 3Y-TZP materials, as well as 4Y-TZP, to compare the results with previous studies and establish a reference point for evaluating the flexural strength of 4Y-TZP. The test results for 3Y-TZP showed a similar tendency to those reported in previous studies. The measured flexural strength of milled 3Y-TZP (Group MZ3) was highest among groups, although the mean value (1045.3±108.7 MPa) was slightly lower than its specification (Katana HT, 1100 MPa). 3D-printed 3Y-TZP (Group PZ3) exhibited significantly lower strength than milled 3Y-TZP (Group MZ3). However, it still exhibited sufficient strength. The flexural strength of PZ3 was found to be 936.8±128.6 MPa, which exceeded the minimum flexural strength requirement of 800 MPa specified in ISO standard 6872 for monolithic ceramics used in prostheses involving partially or fully covered substructures for four or more units. The obtained result was similar to the outcome (943.26±152.75 MPa) reported in Osman et al.'s study, where the same zirconia powder material (TZ-3Y-E, Tosoh, Tokyo, Japan) was

used, and a comparable study design was employed, involving a biaxial flexural strength test by the 'Piston-on-Three-Balls' method.[33]

In contrast, this study found that 3D-printed 4Y-TZP (Group PZ4) had significantly higher flexural strength than milled 4Y-TZP (Group MZ4). Moreover, its flexural strength value (852.4±92.0 MPa) also exceeds 800 MPa, the minimum requirement for multi-unit prosthesis of monolithic ceramic according to ISO 6872. As expected from yttria content, the flexural strength of PZ4 was lower than PZ3, but statistically, there was no significant difference between them.

According to Weibull's weakest link theory, the survival probability of a brittle solid can be calculated as the cumulative product of the survival probabilities of individual volume elements within the solid.[35-37] Some volume elements of the 3D-printed Y-TZP specimen could fail by the limitation of transformation toughening, while others fail due to 3D printing issues. Thus, when enough transformation toughening is allowed, as in 3Y-TZP, many of the elements would fail by weak interlayer bonds than limitation of transformation toughening. On the other hand, when the transformation toughening is not sufficiently allowed, as in 4Y-TZP, more elements would fail due to the limitation of transformation toughening. Therefore, the issues associated with 3D printing of zirconia might not be significant in 4Y-TZP as much as in 3Y-TZP.

The flexural strength of PZ4 was significantly higher than MZ4. One possible explanation for the lower strength of MZ4 is mechanical damage that may have occurred during the milling process. Even though milling pre-sintered zirconia is easier than fully sintered zirconia, it can still cause microcracks or excessive heat that can compromise the strength of the material.[38] As in the case of MZ3, MZ4 also showed lower flexural strength (602.1±70.3 MPa) than its specification (Katana

STML, 750 MPa). It was more profound in MZ4 than in MZ3 and could be attributed to a lower fraction of the tetragonal phase, which endures the mechanical stress by transformation toughening. Another possible factor is the disparity in the yttria content between the two materials. According to the manufacturer's specifications, MZ4 had a yttria content in the 7-10 weight percent range, slightly higher than that of PZ4 (6-8%). It was known that a higher yttria content in Y-TZP increases the fraction of cubic phase, leading to reduced overall strength. For reference, the weight percentage of yttria in 3Y-TZP is approximately 5.2%.[39] In summary, the lower flexural strength of MZ4 compared to PZ4 could be attributed to a combination of factors, including potential mechanical damage during the milling process and the higher yttria content.

The highest Weibull modulus (11.93) was observed in MZ3, while the lowest (8.73) was in PZ3. The higher Weibull modulus in MZ3 is consistent with findings from several previous studies[11, 32], which means that milled 3Y-TZP is more consistent in the strength distribution than 3D-printed 3Y-TZP. Milling is the process of removing from a mass that is uniformly formed. Thus, it is more likely consistent in strength than 3D printing, which accompanies the process of layer bonding.

In contrast, in 4Y-TZP, the Weibull modulus was similar (10.16 in PZ4, 9.98 in MZ4). The group MZ4 showed increased variability in flexural strength than MZ3. It was a possible result since the deleterious effect of the milling process on flexural strength could be more profound in 4Y-TZP due to its lower strength. On the other hand, issues of 3D printing in processing might be less significant in the case of 4Y-TZP, contributing to reduced flexural strength variability in 3D-printed 4Y-TZP. These could contribute to the reduced difference of the Weibull modulus in 4Y-TZP. However, this study investigated only one type of 4Y-TZP material for each

fabrication process; no other relevant studies have been reported. Therefore, further research is necessary.

During the biaxial flexural strength test, specimens exhibited distinctive radial fracture, characterized by radial cracking from the center of the sample toward the edge. It was observed similarly across all groups. Specimens that exhibited higher strength during the test fractured into more fragments, particularly notable in group MZ3. In the study of Inokoshi et al., similar results were identified, which can be attributed to the abrupt release of a higher stored strain energy.[40]

A distinctive pattern considered traces of the milling process was observed in the SEM images of the milled specimens. At a low magnification of x1,000, a regular arrangement of evenly spaced lines accompanied by aligned half circles was visible. At higher magnifications (x20,000), individual grains were identified. The SEM image of MZ3 showed a smaller grain size and a more structurally dense surface than MZ4. This result was similar to Bocam et al.'s study result in the tendency of grain size.[41] In addition, according to Zhang Y and Lawn BR, the typical grain size of 3Y-TZP falls within the range of 0.5 to 1 μm. While, as in 4Y-TZP and 5Y-TZP, increasing the content of yttria and cubic phase could lead to an increase in grain size up to approximately 1.5 μm.[39] In the SEM image of MZ3 and MZ4, many grains had similar grain sizes to those reported in previous studies. In contrast, the 3D-printed group (PZ3, PZ4) showed smooth and consistent surfaces compared to the milled specimens. Grains were not identified on the surface of the 3D-printed specimens but were observed on a cross-sectional image of a fractured segment. PZ3 had a smaller grain size and was more structurally dense than PZ4, as in the milled specimens.

The X-ray diffraction (XRD) patterns showed that the peaks in each group were quite similar and followed a similar pattern. In particular, most of the peaks

corresponded to those of the tetragonal phase of zirconia, as described in the JCPDS-ICDD 014-0534 database. However, the prominent peaks of the cubic phase, which were described in the JCPDS-ICDD 027-0997, were also found to be closely located to the prominent peaks of the tetragonal phase, especially in the vicinity of 30°, 35°, 50° and 60°. Therefore, the observed peaks in this region were super-positioned peaks from both the tetragonal and cubic phase peaks. It suggested that the sample under investigation consisted mainly of a tetragonal phase and some cubic phase.

This study primarily aimed to assess the flexural strength of 3D-printed 4Y-TZP and compare it with milled 4Y-TZP, as well as 3D-printed and milled 3Y-TZP. In addition, SEM and XRD were employed to analyze associated characteristics. The first null hypothesis was rejected, stating that there would be no significant difference in flexural strength between 3D-printed and milled 4Y-TZP. 3D-printed 4Y-TZP had significantly higher flexural strength than milled 4Y-TZP, while 3D-printed 3Y-TZP had lower flexural strength than milled 3Y-TZP as previously reported.

2. Shear bond strength test with surface analysis

Compared with preliminary research[21], this study included surface roughened milled and 3D-printed 4Y-TZP groups via sandblasting to achieve the following objectives. Firstly, to evaluate the impact of sandblasting on the surface and the shear bond strength of veneering porcelain in 3D-printed 4Y-TZP. Secondly, to compare the shear bond strength of veneering porcelain between 3D-printed and milled 4Y-TZP under similarly controlled surface conditions.

The sample number of the shear bond strength test was determined to be fifteen, following ISO 29022:2013.[28] There was no ISO standard for the shear bond strength test for zirconia. Instead, ISO 29022:2013 was used as a reference for the

shear bond strength test since it specifies a shear test method used to determine the adhesive bond strength between direct dental restorative materials and tooth structure.

Thermocycling was done as part of the shear bond strength test to simulate the oral environment considering the limitation of this study as an in-vitro study. The protocol for temperature and dwell time was determined in accordance with ISO/TS 11405:2015.[42] The number of cycling was determined based on previous studies, including literature reviews on thermocycling and adhesion to zirconia.[43, 44]

The veneered porcelain was designed to have a cylindrical form with a diameter of 8mm for ease of reproducibility in size. Since the diameter of the 4Y-TZP specimens was 10mm, a silicon mold with a 10mm inner diameter was used to build up the porcelain consistently. The porcelain had contracted on firing, resulting in a diminished size, still slightly over 8mm. Fine shoulder diamond bur with a 1mm diameter was used to remove any excess material and polish any irregularities, resulting in a final cylindrical form with a diameter of 8±0.1mm.

In addition to veneering porcelain, the shear bond strength for resin cementation was also evaluated in this study. The same study design was maintained in the shear bond strength test for resin cementation to compare the results with each other. Therefore, the size of the resin disk, which was cemented onto the 4Y-TZP specimens by using self-curing resin cement, was also determined as an 8mm diameter.

The surface roughness and wettability were closely related surface characteristics to shear bond strength. Thus, measurements of these properties were also done in evaluating the shear bond strength of 4Y-TZP for resin and veneering porcelain.

The initial surface roughness of 3D-printed 4Y-TZP (PZ4R, Sa: 0.064±0.010 um) was significantly lower than that of milled 4Y-TZP (MZ4R, Sa: 0.358±0.130 um). The measurement was not taken immediately after sintering. Thus, the difference in surface roughness resulted from the fabrication method and post-processing.

Both groups (PZ4S, MZ4S) exhibited a significant increase in surface roughness after sandblasting. The sandblasting process resulted in similar surface roughness and surface profile in both groups despite the initial difference in surface roughness between the two groups (PZ4R, MZ4R). The surface roughness (Sa) was increased to 0.582±0.062 um in PZ4S and 595±0.140 um in MZ4S with sandblasting. The result was similar to the study of Abi-Rached et al., in which a similar sandblasting protocol was used, i.e., sandblasting was done for 15 seconds at a pressure of 0.28 MPa and a perpendicular distance of 10 mm using 50 μm Al_2O_3. Their study reported an increase in the surface roughness (Ra) of zirconia from 0.35 μm to 0.52 μm.[45] Other studies also reported that sandblasting increased the surface roughness of zirconia with a resulting range of 0.3 μm to 1.3 μm, which depends on the particles' size and the pressure utilized during the blasting process.[46-49] According to Inokoshi et al., the effect of sandblasting on the flexural strength of zirconia was determined by the balance between microcrack formation (deteriorating) and surface compressive stress build-up (enhancing). Their study showed that 4Y-TZP (Katana STML) had increased flexural strength after sandblasting with 50um Al_2O_3. Although subsurface microcracks were observed, the generated surface compressive stress compensated for it and enhanced flexural strength.[40] Taken together, these findings suggest that sandblasting is an effective method for increasing surface roughness in zirconia, particularly for surfaces with low surface roughness.

Surface wettability was also increased by sandblasting. The degree of increase depends on the initial surface roughness. Compared with Group PZ4R, the surface free energy of PZ4S was significantly increased. However, the surface free energy of MZ4S was slightly increased compared with MZ4R, but there was no significant difference between them.

The surface free energy of solid, in this study 4Y-TZP, was the sum of the dispersive and polar components. They were calculated from measured contact angles of water and diiodo-methane with the Owens-Wendt & Rable-Kaelble method. Diiodomethane's surface energy is mostly composed of the dispersive component. Therefore, the measured contact angle of diiodomethane is mainly related to the dispersive component of the solid's surface free energy. On the other hand, water's contact angle is more related to the polar component of the surface free energy. The known water's surface free energy is 72.8 mN/m, which consists of 51.0 mN/m of the polar component and 21.8 mN/m of the dispersive component.[50]

The water contact angle of group PZ4R was significantly higher than group PZ4S, indicating that the roughened surface by sandblast leads to a decrease in water contact angle. However, in the case of group MZ4R, there was no significant difference in water contact angle compared to MZ4S. It suggests that beyond a certain level of surface roughness, further increases may not significantly reduce the water contact angle. This finding is consistent with a previous study conducted by Kwon et al.[51] In their study, sandblasting on polished zirconia caused a notable decrease in the water contact angle (when Ra increased from 0.04 um to 0.63 um, the water contact angle reduced from 59.7° to 44.1°). However, when Ra was increased to 1.06 um by aggressive sandblasting protocol with higher pressure and large particle, the reduced water contact angle was not so much different, with a

value of 40.9°. On the other hand, MZ4S showed a slightly lower water contact angle than PZ4S, but no significant difference existed between them. Thus, no significant difference was found between 3D-printed 4Y-TZP and milled 4Y-TZP in the polar surface energy when they had similar surface roughness.

Differently, in the case of water contact angle, the contact angle of diiodo-methane was significantly reduced by sandblast in both groups, i.e., there were significant differences between MZ4R and MZ4S, as well as between PZ4R and PZ4S. However, there were no significant differences found between 3D-printed and Milled 4Y TZP, regardless of sandblasting. No significant difference was found between PZ4R (52.10±2.20°) and MZ4R (50.07±2.86°), as well as PZ4S (37.32±0.96°) and MZ4S (37.56±2.54°). There was a significant difference in surface roughness between PZ4R (Sa: 0.064±0.010 um) and MZ4R (Sa: 0.358±0.130 um), like PZ4R and PZ4S (Sa: 0.582±0.062 um) or MZ4R and MZ4S (Sa: 0.595±0.140 um), but the contact angle of diiodo-methane was not significantly different. The findings indicate that, up to a certain threshold, the surface roughness had minimal impact on the contact angle of diiodo-methane. However, above this level, the influence of surface roughness increased, and the contact angle of diiodo-methane was notably reduced in proportion to the surface roughness. It indicates that 4Y-TZP's dispersion component of surface free energy increased correspondingly with the increased surface roughness. Rudawska et al. reported that an increase in surface roughness by sandblast leads to a proportional increase in the dispersive component of surface free energy, similar to this study.[52]

In essence, the surface wettability of 4Y-TZP was affected by surface roughness. Increased surface roughness by sandblast resulted in a significant decrease of the

water contact angle within the range of low surface roughness. However, beyond a certain level of surface roughness, further increases in surface roughness did not significantly reduce the water contact angle, which mainly relates polar component of surface free energy. In contrast, the influence of surface roughness on the dispersion component of surface free energy of 4Y-TZP was increased correspondingly with the increased surface roughness. There was no difference in surface energy between 3D printed and milled 4Y-TZP with similar surface roughness. However, this study result should be used and interpreted cautiously due to factors such as the susceptibility of contact angle measurements to laboratory conditions (e.g., humidity, temperature)[30], limitations in sample size, and insufficient supporting studies.

There was a significant difference in the shear bond strength of veneering porcelain between 3D-printed 4Y-TZP and milled 4Y-TZP. However, with similar surface roughness via sandblasting, they showed no significant difference in the shear bond strength of porcelain. It means that 3D-printed and milled 4Y-TZP had a comparable surface binding ability to porcelain if they had similar surface roughness.

The shear bond strength was significantly increased by sandblast in 3D-printed 4Y-TZP, which has low surface roughness and surface wettability. In contrast, in milled 4Y-TZP, it slightly increased but not remarkably, and this tendency was similar to the study results of surface energy. These results suggest that as surface energy, shear bond strength in porcelain was also affected by surface roughness, and they were closely related.

The measured shear bond strength of veneered porcelain was relatively low compared to previous studies.[13, 53, 54] The factors that affect the bond strength

between zirconia and veneering porcelain include surface roughness, mismatch of thermal expansion coefficient, flaws or structural defects in the interface, wetting properties, and volumetric shrinkage of the veneered porcelain.[53, 55] The extent to which these factors affect the shear bond strength can vary depending on the methodology and protocol used in the study design. Based on the study design, the most probable cause of the observed low shear bond strength in this study was flaws and structural defects. It is likely because, compared to previous studies[13, 53, 54], the veneered surface area in this study was wider. With porcelain building up being a technique-sensitive process, the larger surface area increases the likelihood of structural defects occurring at the interface. Still, in the clinical situation, zirconia crowns used in anterior restorations were commonly veneered by porcelain due to esthetic needs. In such cases, the expected binding area is often more extensive than in the model used in this study. Therefore, these study results could still be referenceable and provide some insights into the potential challenges and factors that may affect the success of veneered zirconia crowns in clinical settings.

The Weibull modulus of the PZ4R group was higher than other groups. One reason might be related to the fracture pattern observed in the specimens. PZ4R specimens showed mixed failure patterns but were close to adhesive failure patterns with a small amount of porcelain remaining. The other groups with higher shear bond strength also displayed mixed failure patterns. However, they were more likely to cohesive failure, with many portions of the fracture surface covered by a sheet of porcelain remnant. Since cohesive failure occurred not in the ceramic-zirconia interface where the load was applied but within the ceramic, the failure strength is more likely variable than in the case of adhesive failure. Another possible factor is the use of PMMA to embed the specimens. As the applied shear

bond strength increases, there is a risk that microfractures may occur at the interface between the PMMA and the zirconia specimen. This could lead to unstable shear loading to the specimen and potentially contribute to the observed variability in shear bond strength measurements. Thus, to minimize this potential source of error, it may be considerable to use a more rigid or firm material for embedding specimens, particularly in situations where a higher shear bond strength is expected.[53]

This study also evaluated the shear bond strength for resin cementation. The shear bond strength measured in this study (3.33±0.98 in PZ4S, 3.25±0.83 in MZ4S) was lower compared to previous studies[43] but higher than a recently reported study (1.50±0.51) that employed similar experimental designs, including the use of the same self-adhesive resin cement, sandblasting, and thermocycling protocol[56]. Several study design factors influenced the measured shear bond strength of zirconia adhesion, such as surface treatment methods, cement types, aging protocols, and test methods. In previous studies, the study utilizing a physicochemical surface treatment and MDP-based cement without an aging protocol reported higher shear bond strength.[43] Although physicochemical treatment was done by sandblasting and applying zirconia primer, both groups (PZ4S, MZ4S) still showed low shear bond strength in this study. The use of self-adhesive resin cement instead of MDP-based cement, the thermocycling procedure, and a larger adhesion area were possible contributing factors for low shear bond strength.

The shear bond strength was approximately one-fourth of that observed in veneering porcelain compared to the same study design. These results, with their low Weibull modulus, indicate that adhesion to zirconia is still weak and unreliable.

Again, as in veneering porcelain, with similar surface roughness, there was no significant difference in the shear bond strength of resin cementation.

The second null hypothesis, which states no significant difference in shear bond strength and surface characteristics between 3D-printed and milled 4Y-TZP, was partially rejected based on the presented results. The study found a significant difference in the shear bond strength of porcelain and surface characteristics between 3D-printed and milled 4Y-TZP. However, there was no significant difference between the two groups in surface wettability and shear bond strength of veneering porcelain and resin cementation when they had similar surface roughness by sandblasting.

V. CONCLUSIONS

Within the limitations of this study, the results suggest the following conclusions.

1. The flexural strength of 3D-printed 4Y-TZP was significantly higher than milled 4Y-TZP.
2. 3D-printed 4Y-TZP showed significantly lower shear bond strength of veneering porcelain than milled 4Y-TZP due to lower surface roughness and surface energy.
3. Surface roughness and surface energy of 3D-printed 4Y-TZP significantly increased after sandblasting.
4. 3D-printed 4Y-TZP had similar shear bond strength for veneering porcelain and resin cementation with milled 4Y-TZP when they had equivalent surface roughness and surface energy with sandblasting.

Conclusively, 3D-printed 4Y-TZP could be the preferable material for zirconia restoration with clinically acceptable flexural strength and shear bond strength compared to milled 4Y-TZP.

REFERENCES

1. Grech J, Antunes E. Zirconia in dental prosthetics: A literature review. J Mater Res Technol. 2019;8(5):4956-64.
2. Mazza LC, Lemos CAA, Pesqueira AA, Pellizzer EP. Survival and complications of monolithic ceramic for tooth-supported fixed dental prostheses: A systematic review and meta-analysis. J Prosthet Dent. 2022;128(4):566-74.
3. Al-Amleh B, Lyons K, Swain M. Clinical trials in zirconia: a systematic review. J Oral Rehabil. 2010;37(8):641-52.
4. Abduo J, Lyons K, Bennamoun M. Trends in computer-aided manufacturing in prosthodontics: a review of the available streams. Int J Dent. 2014;2014:783948. doi: 10.1155/2014/783948. Epub 2014 Apr 8.
5. Leeson D. The digital factory in both the modern dental lab and clinic. Dent Mater. 2020;36(1):43-52.
6. Watanabe H, Fellows C, An H. Digital Technologies for Restorative Dentistry. Dent Clin North Am. 2022;66(4):567-90.
7. Huang H. Machining characteristics and surface integrity of yttria stabilized tetragonal zirconia in high speed deep grinding. Mater Sci Eng: A. 2003;345(1):155-63.
8. Methani MM, Revilla-León M, Zandinejad A. The potential of additive manufacturing technologies and their processing parameters for the fabrication of all-ceramic crowns: A review. J Esthet Restor Dent. 2020;32(2):182-92.
9. Revilla-León M, Meyer MJ, Zandinejad A, Özcan M. Additive manufacturing technologies for processing zirconia in dental applications. Int J Comput Dent. 2020;23(1):27-37.

10. Suominen JM, Frankberg EJ, Vallittu PK, Levänen E, Vihinen J, Vastamäki T, et al. Three-dimensional printing of zirconia: characterization of early stage material properties. Biomater Investig Dent. 2019;6(1):23-31.
11. Revilla-León M, Al-Haj Husain N, Ceballos L, Özcan M. Flexural strength and Weibull characteristics of stereolithography additive manufactured versus milled zirconia. J Prosthet Dent. 2021;125(4):685-90.
12. Valenti C, Isabella Federici M, Masciotti F, Marinucci L, Xhimitiku I, Cianetti S, et al. Mechanical properties of 3D-printed prosthetic materials compared with milled and conventional processing: A systematic review and meta-analysis of in vitro studies. J Prosthet Dent. 2022 Aug 5:S0022-3913(22)00415-2. doi: 10.1016/j.prosdent.2022.06.008. Epub ahead of print.
13. Baysal N, Tuğba Kalyoncuoğlu Ü, Ayyıldız S. Mechanical Properties and Bond Strength of Additively Manufactured and Milled Dental Zirconia: A Pilot Study. J Prosthodont. 2022;31(7):629-34.
14. Abualsaud R, Abussaud M, Assudmi Y, Aljoaib G, Khaled A, Alalawi H, et al. Physiomechanical and Surface Characteristics of 3D-Printed Zirconia: An In Vitro Study. Materials (Basel). 2022;15(19):6988. doi: 10.3390/ma15196988.
15. Bergler M, Korostoff J, Torrecillas-Martinez L, Mante FK. Ceramic Printing - Comparative Study of the Flexural Strength of 3D Printed and Milled Zirconia. Int J Prosthodont. 2022;35(6):777–83.
16. Zhang F, Inokoshi M, Batuk M, Hadermann J, Naert I, Van Meerbeek B, et al. Strength, toughness and aging stability of highly-translucent Y-TZP ceramics for dental restorations. Dent Mater. 2016;32(12):e327-37.
17. Carrabba M, Keeling AJ, Aziz A, Vichi A, Fabian Fonzar R, Wood D, et al. Translucent zirconia in the ceramic scenario for monolithic restorations: A

flexural strength and translucency comparison test. J Dent. 2017;60:70-6.

18. Jerman E, Lümkemann N, Eichberger M, Zoller C, Nothelfer S, Kienle A, et al. Evaluation of translucency, Marten's hardness, biaxial flexural strength and fracture toughness of 3Y-TZP, 4Y-TZP and 5Y-TZP materials. Dent Mater. 2021;37(2):212-22.
19. Jansen JU, Lümkemann N, Letz I, Pfefferle R, Sener B, Stawarczyk B. Impact of high-speed sintering on translucency, phase content, grain sizes, and flexural strength of 3Y-TZP and 4Y-TZP zirconia materials. J Prosthet Dent. 2019;122(4):396-403.
20. Schönhoff LM, Lümkemann N, Buser R, Hampe R, Stawarczyk B. Fatigue resistance of monolithic strength-gradient zirconia materials. J Mech Behav Biomed Mater. 2021;119:104504. doi: 10.1016/j.jmbbm.2021.104504. Epub 2021 Apr 7.
21. Kyung KY, Koak JY, Kim SK, Park JM, Heo SJ. Comparative study of surface characteristics and shear bond strength of 3D printed and milled 4Y-TZP. Korean J Dent Mater. 2023;50(1):69-80.
22. International Organization for Standardization. ISO 6872:2015. Dentistry-Ceramic materials. Geneva: International Organization for Standardization; 2015.
23. Blom G. Statistical estimates and transformed beta-variables: Almqvist & Wiksell; 1958.
24. Davies IJ. Unbiased estimation of Weibull modulus using linear least squares analysis—A systematic approach. J Eur Ceram Soc. 2017;37(1):369-80.
25. McMurdie HF, Morris MC, Evans EH, Paretzkin B, Wong-Ng W, Hubbard CR. Standard X-Ray Diffraction Powder Patterns from The JCPDS Research Associateship. Powder Diffr. 1986;1:275.

26. L. N. Komissarova LN, Simanov YP, Vladimirova ZA. Russ J Inorg Chem (Engl. Transl.). 1960;5:687.
27. Katz G. X-Ray Diffraction Powder Pattern of Metastable Cubic ZrO2. J Am Ceram Soc. 1971;54:531.
28. International Organization for Standardization. ISO 29022:2013. Dentistry-Adhesion-Notched-egde shear bond strength test. Geneva: International Organization for Standardization; 2013.
29. Owens DK, Wendt RC. Estimation of the surface free energy of polymers. J Appl Polym Sci. 1969;13(8):1741-7.
30. Rudawska A, Jacniacka E. Analysis for determining surface free energy uncertainty by the Owen–Wendt method. Int J Adhes Adhes. 2009;29(4):451-7.
31. Quinn JB, Quinn GD. A practical and systematic review of Weibull statistics for reporting strengths of dental materials. Dent Mater. 2010;26:135-47.
32. Revilla-León M, Al-Haj Husain N, Barmak AB, Pérez-López J, Raigrodski AJ, Özcan M. Chemical Composition and Flexural Strength Discrepancies Between Milled and Lithography-Based Additively Manufactured Zirconia. J Prosthodont. 2022;31(9):778-83.
33. Osman RB, van der Veen AJ, Huiberts D, Wismeijer D, Alharbi N. 3D printing zirconia implants; a dream or a reality? An in-vitro study evaluating the dimensional accuracy, surface topography and mechanical properties of printed zirconia implant and discs. J Mech Behav Biomed Mater. 2017;75:521-8.
34. Zocca A, Colombo P, Gomes CM, Günster J. Additive Manufacturing of Ceramics: Issues, Potentialities, and Opportunities. J Am Ceram Soc. 2015;98(7):1983-2001.
35. Zok FW. On weakest link theory and Weibull statistics. J Am Ceram Soc.

2017;100(4):1265-8.

36. Weibull W. A statistical theory of the strength of materials. Royal Inst for Eng Res, Stockholm. 1939;151:1–45.
37. Weibull W. A Statistical Distribution Function of Wide Applicability. J Appl Mech. 1951;18(3):293-7.
38. Yin Y, Xu J, Ji M, Li L, Chen M. A critical review on sintering and mechanical processing of 3Y-TZP ceramics. Ceram Int. 2023;49(2):1549-71.
39. Zhang Y, Lawn BR. Novel Zirconia Materials in Dentistry. J Dent Res. 2018;97(2):140-7.
40. Inokoshi M, Shimizubata M, Nozaki K, Takagaki T, Yoshihara K, Minakuchi S, et al. Impact of sandblasting on the flexural strength of highly translucent zirconia. J Mech Behav Biomed Mater. 2021;115:104268. doi: 10.1016/j.jmbbm.2020.104268. Epub 2020 Dec 13.
41. Bocam K, Anunmana C, Eiampongpaiboon T. Grain size, crystalline phase and fracture toughness of the monolithic zirconia. J Adv Prosthodont. 2022;14(5):285-93.
42. International Organization for Standardization. ISO/TS 11405:2015. Dentistry-Testing of adhesion to tooth structure. Geneva: International Organization for Standardization; 2015.
43. Özcan M, Bernasconi M. Adhesion to Zirconia Used for Dental Restorations: A Systematic Review and Meta-Analysis. J Adhes Dent. 2015;17(1):7-26.
44. Morresi AL, D'Amario M, Capogreco M, Gatto R, Marzo G, D'Arcangelo C, et al. Thermal cycling for restorative materials: Does a standardized protocol exist in laboratory testing? A literature review. J Mech Behav Biomed Mater. 2014;29:295-308.

45. Abi-Rached FO, Martins SB, Campos JA, Fonseca RG. Evaluation of roughness, wettability, and morphology of an yttria-stabilized tetragonal zirconia polycrystal ceramic after different airborne-particle abrasion protocols. J Prosthet Dent. 2014;112(6):1385-91.
46. Finger C, Stiesch M, Eisenburger M, Breidenstein B, Busemann S, Greuling A. Effect of sandblasting on the surface roughness and residual stress of 3Y-TZP (zirconia). SN Appl Sci. 2020;2(10):1700.
47. He M, Zhang Z, Zheng D, Ding N, Liu Y. Effect of sandblasting on surface roughness of zirconia-based ceramics and shear bond strength of veneering porcelain. Dent Mater J. 2014;33(6):778-85.
48. Nakamura T, Wakabayashi K, Zaima C, Nishida H, Kinuta S, Yatani H. Tensile bond strength between tooth-colored porcelain and sandblasted zirconia framework. J Prosthodont Res. 2009;53(3):116-9.
49. Liu D, Matinlinna JP, Tsoi JK-H, Pow EHN, Miyazaki T, Shibata Y, et al. A new modified laser pretreatment for porcelain zirconia bonding. Dent Mater. 2013;29(5):559-65.
50. Jańczuk B, Białłopiotrowicz T. Surface free-energy components of liquids and low energy solids and contact angles. J Colloid Interface Sci. 1989;127(1):189-204.
51. Kwon SM, Min BK, Kim YK, Kwon TY. Influence of Sandblasting Particle Size and Pressure on Resin Bonding Durability to Zirconia: A Residual Stress Study. Materials (Basel). 2020;13(24):5629. doi: 10.3390/ma13245629.
52. Rudawska A, Danczak I, Müller M, Valasek P. The effect of sandblasting on surface properties for adhesion. Int J Adhes Adhes. 2016;70:176-90.
53. Choi BK, Han JS, Yang JH, Lee JB, Kim SH. Shear bond strength of veneering

porcelain to zirconia and metal cores. J Adv Prosthodont. 2009;1(3):129-35.

54. Ozkurt Z, Kazazoglu E, Unal A. In vitro evaluation of shear bond strength of veneering ceramics to zirconia. Dent Mater J. 2010;29(2):138-46.

55. Isgrò G, Pallav P, van der Zel JM, Feilzer AJ. The influence of the veneering porcelain and different surface treatments on the biaxial flexural strength of a heat-pressed ceramic. J Prosthet Dent. 2003;90(5):465-73.

56. Serichetaphongse P, Chitsutheesiri S, Chengprapakorn W. Comparison of the shear bond strength of composite resins with zirconia and titanium using different resin cements. J Prosthodont Res. 2022;66(1):109-16.

국문초록

3차원 프린팅으로 제작된 4몰 이트리아 안정화 지르코니아의 굴곡파절강도 및 표면 분석을 동반한 전단결합강도의 연구

서울대학교 대학원 치의과학과 치과보철학 전공

(지도교수 허 성 주)

경 규 영

목 적 : 본 연구의 목적은 첫째로 3 차원 프린팅으로 제작된 4 몰 이트리아 안정화 지르코니아(4Y-TZP) 시편의 굴곡파절강도를 평가하는 것이다. 두번째 목적은 표면 분석을 바탕으로 도재 및 레진합착에 대한 전단결합강도를 평가하는 것이다.

재료 및 방법 : 굴곡파절강도 실험을 위해서 직경 15mm, 두께 1.5mm 크기의 이트리아 안정화 지르코니아 원판형 시편을 총 80 개 제작하였다. 시편들은 제작 방식과 이트리아 함량에 따라 절삭가공으로 제작된 3Y (Katana HT, Kuraray Noritake, Tokyo, Japan) 및 4Y-TZP (Katana

STML, Kuraray Noritake, Tokyo, Japan)군 및 3 차원 프린팅으로 제작된 3Y (TZ-3Y-E, Tosoh, Tokyo, Japan) 및 4Y-TZP (3DMAT, Genoss, Suwon, Korea)군의 4 개의 군으로 분류하였다. 이축 굴곡강도 시험은 'Piston-on-Three-Ball' 방법을 이용하여 수행하였다(n=15). 굴곡파절강도의 측정과 더불어 측정된 파절강도의 분포로부터 와이블 계수 및 특성강도를 추정하였다. 주사전자현미경으로 시편 표면 및 파절편의 단면을 관찰하였고(n=2), X 선 회절분석을 통해서 각 군 시편의 주된 결정상을 확인하였다(n=5).

전단결합강도 실험을 위해서 직경 10mm, 두께 1.2mm 크기의 4Y-TZP 시편을 3 차원 프린팅 및 절삭가공 방식으로 총 90 개 제작하였다. 도재 전장 및 레진 시멘트 합착에 대한 전단결합강도 실험을 수행하였으며, 도재 전장에 대한 전단결합강도 실험은 샌드블라스팅 처리가 이루어진 군과 이루어지지 않은 군 모두에 대해 각각 진행하였다. 각 전단결합강도 실험에 대한 군당 시편 수는 15 개로 하였다. 도재 전장에 대한 전단결합강도 측정을 위해서 4Y-TZP 시편 표면에 장석 도재 (CZR dentin powder, Kuraray Noritake, Tokyo, Japan)를 원판형태로 축성 및 소성하였다. 레진 시멘트 합착에 대한 전단결합강도 실험시에는 3 차원 프린팅 및 절삭가공으로 제작된 4Y-TZP 시편 표면에 샌드블라스팅, 에칭 처리 및 금속/지르코니아 프라이머 (Metal Primer Z, GC, Tokyo, Japan)를 적용 후 자가중합 레진 시멘트 (Rely X U200, 3M ESPE, Saint Paul, MN, USA)를 이용하여 원판형 복합 레진 (Gradia Direct Anterior, GC, Tokyo, Japan) 디스크를 합착하였다.

전단결합강도 시편에 대한 표면분석을 시행하였다 (n=5). 3 차원 공초점 레이저 주사 현미경을 이용하여 표면조도를 측정하였다. 표면에너지는 물과 디아이오도 메탄의 접촉각으로 부터 ‘Owens-Wendt & Rable-Kaelble’ 법을 이용하여 산출하였다.

자료에 대한 통계처리는 통계분석 프로그램 (SPSS version 26, IBM Corp, Armonk, NY, USA)을 이용하여 수행하였다. Shapiro-Wilk 검정법을 이용하여 자료의 정규성을 검증하였다. 군들 간에서 자료의 유의성 여부를 확인하기 위해 정규성 여부와 표본크기에 따라 일원분산분석 또는 Kruskal-Wallis 검정을 시행하였으며, 유의성이 확인된 경우, 각 군간 사후분석을 수행하였다. 일원분산분석에 대해서는 Tukey 의 사후검정, Kruskal-Wallis 검정에 있어서는 Mann-Whitney U 검정을 적용하였다.

결 과 : 3차원 프린팅으로 제작된 4Y-TZP는 절삭가공으로 제작된 4Y-TZP와 비교하여 유의미하게 높은 굴곡파절강도를 보였다($P<.001$). 반면 3차원 프린팅으로 제작된 3Y-TZP는 절삭가공으로 제작된 3Y-TZP보다 유의미하게 낮은 굴곡파절강도를 보였다($P<.001$). X선 회절분석결과 정방정계상(Tetragonal phase)이 모든 군에서 주된 상으로 나타났으며, 일부 입방정계상(Cubic phase)의 피크가 확인되었다.

3차원 프린팅으로 제작된 4Y-TZP는 절삭가공으로 제작된 4Y-TZP와 비교하였을 때 유의하게 낮은 표면조도(Sa, Sq)를 보였다($P<.001$). 샌드블라스팅으로 표면처리를 시행하였을 때, 두 군 모두 이전과 비교하여 표면 조도에서 유의한 증가를 보였다($P<.001$). 그러나 샌드블라스팅 처리된

두 군 사이에는 통계적으로 유의미한 차이를 보이지 않았다(Sa: P=.877, Sq: P=.915).

물과 디아이오도메탄에 대한 접촉각 측정으로부터 산출된 표면에너지를 비교하였을 때, 3 차원 프린팅으로 제작된 4Y-TZP 는 절삭가공으로 제작된 4Y-TZP 와 비교하여 유의미하게 낮은 표면에너지를 보였다(P=.008). 그러나 샌드블라스팅 처리 후에는 두 군 사이에 표면에너지에 있어 유의한 차이는 없었다(P=.056). 샌드블라스팅 처리 후 3 차원 프린팅으로 제작된 4Y-TZP 는 유의한 표면에너지의 증가를 보였다(P=.008). 반면에, 절삭가공으로 제작된 4Y-TZP 는 처리 전과 비교하여 통계적으로 유의미한 차이가 없었다 (P=.095).

도재 전장에 대한 전단결합강도 비교에 있어 3 차원 프린팅으로 제작된 4Y-TZP 는 절삭가공으로 제작된 4Y-TZP 와 비교하여 유의하게 낮은 전단결합강도를 보였다(P<.001). 그러나 샌드블라스팅으로 표면처리 한 후에는 두 군 사이에 유의한 차이가 관찰되지 않았으며(P=.412), 3 차원 프린팅으로 제작된 4Y-TZP 는 샌드블라스팅 처리에 의해 전단결합강도가 유의미하게 증가한 반면(P<.001), 절삭가공으로 제작된 4Y-TZP 는 통계적 유의미한 증가를 보이지 않았다(P=.116). 레진시멘트 합착에 대한 전단결합강도는 3 차원 프린팅으로 제작된 4Y-TZP 와 절삭가공으로 제작된 4Y-TZP 사이에 유의한 차이가 없었다(P=.811).

결 론 : 본 연구의 한계 내에서 통계적 분석을 통해 내린 결론은 다음과 같다.

1. 3 차원 프린팅으로 제작된 4Y-TZP 는 절삭가공으로 제작된 4Y-TZP 와 비교하여 유의미하게 높은 굴곡파절강도를 보였다.
2. 3 차원 프린팅으로 제작된 4Y-TZP 는 절삭가공으로 제작된 4Y-TZP 와 비교하여 도재 전장에 있어 유의미하게 낮은 전단결합강도를 보였으며, 이는 낮은 표면조도와 표면에너지에서 기인한다.
3. 3 차원 프린팅으로 제작된 4Y-TZP 표면에 샌드블라스팅 처리시 표면조도와 표면에너지가 유의미하게 증가하였다.
4. 3 차원 프린팅 및 절삭가공으로 제작된 4Y-TZP 는 샌드블라스팅 처리시 유사한 표면조도 및 표면에너지를 보였으며, 이 때 도재 전장 및 레진 합착에 대한 전단결합강도에서 차이를 보이지 않았다.

결론하여, 3 차원 프린팅으로 제작된 4Y-TZP 는 임상적으로 적합한 굴곡파절강도와 전단결합강도를 보였으며, 절삭가공방식으로 제작된 4Y-TZP 와 비교하여 지르코니아 수복에 있어 보다 선호되는 재료가 될 수 있다 사료된다.

주요어: Y-TZP, 3D 프린팅, 굴곡파절강도, 전단결합강도, 표면조도

학 번: 2018-39754

감사의 글

박사과정을 무사히 마치고 이 논문을 시작하여 마무리하기까지 많은 도움을 주신 여러 스승님과 동료, 가족에게 감사의 말씀을 전합니다.

치과보철과 전임의 및 대학원 생활에 있어 따듯한 충고와 조언으로 진료와 연구에 귀중한 가르침을 주신 허성주 교수님께 깊은 감사를 드립니다. 병원 진료와 업무로 바쁘신 와중에도 본 논문을 위하여 많은 지도 편달을 해 주셨습니다.

국소의치학이라는 학문의 깊이와 열정을 일깨워주시고, 본 논문 심사와 지도에 열과 성을 다해주신 곽재영 교수님, 김성균 교수님, 박지만 교수님께도 깊은 감사를 드립니다.

바쁘신 와중에도 본 논문 심사를 위하여 꼼꼼히 살펴주신 경희대학교 치과대학의 김형섭 교수님과 치과생체재료과학교실의 안진수 교수님께도 감사드립니다.

항상 격려와 조언을 아끼지 않으신 치과보철학교실의 한중석 명예교수님, 임영준 교수님, 권호범 교수님, 김명주 교수님, 여인성 교수님, 윤형인 교수님, 이재현 교수님과 치과보철학 교실원 여러분께 이 자리를 빌려 감사의 말씀을 전합니다.

치과보철과 수련기간 동안 지도해주신 아산병원 김종진 교수님, 이주희 교수님, 백진 교수님, 차현석 교수님과 동고동락한 의국 선후배님들께도 감사의 말씀을 전합니다.

치과대학생부터 오늘에 이르기까지 많은 관심으로 격려해주시는 구강악안면외과학교실의 김성민 교수님께 깊이 감사드립니다.

마지막으로, 오늘의 제가 있기까지 많은 사랑과 정성으로 보살펴주시고 지원해주신 양가 부모님께 깊은 감사를 드리며, 제가 하는 모든 일을 응원해주는 배정윤과, 경민서에게도 고마움을 전합니다.

2023 년 8 월

경 규 영